Precambrian olistoliths masquerading as sills from Death Valley, California

Vandyk, Thomas; Le Heron, Daniel P.; Chew, David; Amato, Jeff; Thirlwall, Matthew; Dehler, Carol; Hennig, Juliane; Castonguay, Samuel; Knott, Tom; Tofaif, Saeed; Ali, Dilshad; Manning, Christina; Busfield, Marie; Doepke, Daniel; Grassineau, Nathalie

Published in:
Journal of the Geological Society

DOI:
10.1144/jgs2017-002

Publication date:
2018

Citation for published version (APA):
Vandyk, T., Le Heron, D. P., Chew, D., Amato, J., Thirlwall, M., Dehler, C., Hennig, J., Castonguay, S., Knott, T., Tofaif, S., Ali, D., Manning, C., Busfield, M., Doepke, D., & Grassineau, N. (2018). Precambrian olistoliths masquerading as sills from Death Valley, California. *Journal of the Geological Society*, *175*(3), 377-395. [jgs2017-002]. https://doi.org/10.1144/jgs2017-002

JGS
Journal of the Geological Society

Research article

Published Online First

https://doi.org/10.1144/jgs2017-002

Precambrian olistoliths masquerading as sills from Death Valley, California

T. M. Vandyk[1]*, D. P. Le Heron[1], D. M. Chew[2], J. M. Amato[3], M. Thirlwall[1], C. M. Dehler[4], J. Hennig[1], S. R. Castonguay[5], T. Knott[6], S. Tofaif[1], D. O. Ali[1], C. J. Manning[1], M. E. Busfield[7], D. Doepke[2] & N. Grassineau[1]

[1] Department of Earth Sciences, Royal Holloway University of London, Queen's Building, Egham TW20 0EX, UK
[2] Department of Geology, Trinity College Dublin, Museum Building, Dublin 2, Ireland
[3] Department of Geological Sciences, New Mexico State University, Las Cruces, NM 88003, USA
[4] Department of Geology, Utah State University, 4505 Old Main Hill, Logan, UT 84322-4505, USA
[5] Treasure Valley Community College, 650 College Blvd., Ontario, OR 97914, USA
[6] Department of Geology, University of Leicester, University Road, Leicester LE1 7RH, UK
[7] Department of Geography & Earth Sciences, Aberystwyth University, Llandinam Building, Penglais Campus, Aberystwyth SY23 3DB, UK

T.M.V., 0000-0002-7732-9977; D.M.C., 0000-0002-6940-1035; J.M.A., 0000-0001-5742-6115; T.K., 0000-0002-6453-7486; S.T., 0000-0003-3241-1261; D.D., 0000-0003-4850-9474

*Correspondence: Thomas.Vandyk.2016@live.rhul.ac.uk

Abstract: Olistolith production and magmatism are processes commonly associated with extensional tectonic settings, such as rift basins. We present a cautionary exemplar from one such Precambrian basin, in which we reinterpret metabasite bodies, previously documented as sills, to be olistoliths. We nevertheless demonstrate that, on the basis of field observation alone, the previous but erroneous sill interpretation is parsimonious. Indeed, it is only by using isotopic age and compositional analysis that the true identities of these metabasite olistoliths are revealed. We present new data from metabasites and metasedimentary strata of the Kingston Peak Formation (Cryogenian) and Crystal Spring Formation (Mesoproterozoic) of Death Valley, USA. These include field observations, U–Pb apatite ages, U–Pb zircon ages (detrital and igneous) and whole-rock geochemistry. These data also provide a new maximum age for the base of the Pahrump Group and suggest that the Crystal Spring Diabase was more tholeiitic than previously thought. Similar sill/olistolith misinterpretations may have occurred elsewhere, potentially producing erroneous age and tectonic-setting interpretations of surrounding strata. This is particularly relevant in Precambrian rocks, where fossil age constraints are rare. This is illustrated herein using a potential example from the Neoproterozoic literature of the Lufilian belt, Africa. We caution others against Precambrian olistoliths masquerading as sills.

Supplementary material: Details of a meta-igneous boulder from P12 of the Silurian Hills, LA-ICP-MS and whole-rock geochemistry methods and standards, and U–Pb apatite and zircon isotopic data, including standards and selected cathodoluminescence images, are available at https://doi.org/10.6084/m9.figshare.c.3990639

Received 9 January 2017; **revised** 17 December 2017; **accepted** 21 December 2017

Extensional tectonic settings, such as rift basins, are often associated with the production of intrusive magmas (e.g. Tembo *et al*. 1999) and with slope failure. The latter may result in the formation and transport of bedrock megaclasts, from tens of metres to kilometres in size, known as olistoliths (Festa *et al*. 2012). This study provides a cautionary exemplar in which these two inherently linked processes had become confused. Mafic intrusions emplaced during a *c.* 1.1 Ga rift episode were remobilized >300 myr later as olistoliths. They were, however, misidentified, both in the literature and more recently by the authors of this study, as *in situ* sills (Kupfer 1960; Basse 1978; Shapiro *et al*. 2014). Such misidentification might occur elsewhere and with significant implications. First, radiometric dates obtained from an igneous body may be incorrectly interpreted, as minimum rather than maximum ages for the enclosing strata. This is especially pertinent in Precambrian successions, as fossil dating is rarely applicable. Second, the geochemistry of an olistolith may be erroneously used to constrain the tectonic setting of enclosing strata, if it is believed to be an *in situ* sill.

This study focuses on misinterpreted metabasite bodies, from within the Cryogenian Kingston Peak Formation (KPu) of the Silurian Hills, near Death Valley, USA (Fig. 1). The KPu preserves an archive of rifting, glaciation and magmatism (Hazzard 1939; Labotka *et al*. 1980; Hammond 1983; Miller 1985; Prave 1999; Le Heron *et al*. 2014). The 'Zipper-Rift' model of Eyles & Januszczak (2004) suggested that there was a causal relationship between rifting and the pervasive glaciation of the Cryogenian. In contrast, Li *et al*. (2013) questioned the importance of this process, arguing that there was not a straightforward relationship between diamictite distribution and palaeo-rift location. Olistoliths are well established within the KPu of the Goler Wash (Panamint Range), Kingston Range and Silurian Hills areas (Fig. 1) (Miller 1985; Walker *et al*. 1986; Prave 1999; Calzia *et al*. 2000; Macdonald *et al*. 2013; Le Heron *et al*. 2014, 2018). Globally, olistostromes only rarely occur within Neoproterozoic glacial successions (e.g. Baykonur Fm; Chumakov 2011). The Silurian Hills are therefore unusual in containing multiple olistostrome packages, enclosed by glacial strata both above and below (Le Heron *et al*. 2017).

Geological setting

In ascending stratigraphic order, the Pahrump Group consists of the Crystal Spring Formation, Horse Thief Springs Formation, Beck Spring Dolomite and Kingston Peak Formation (KPu).

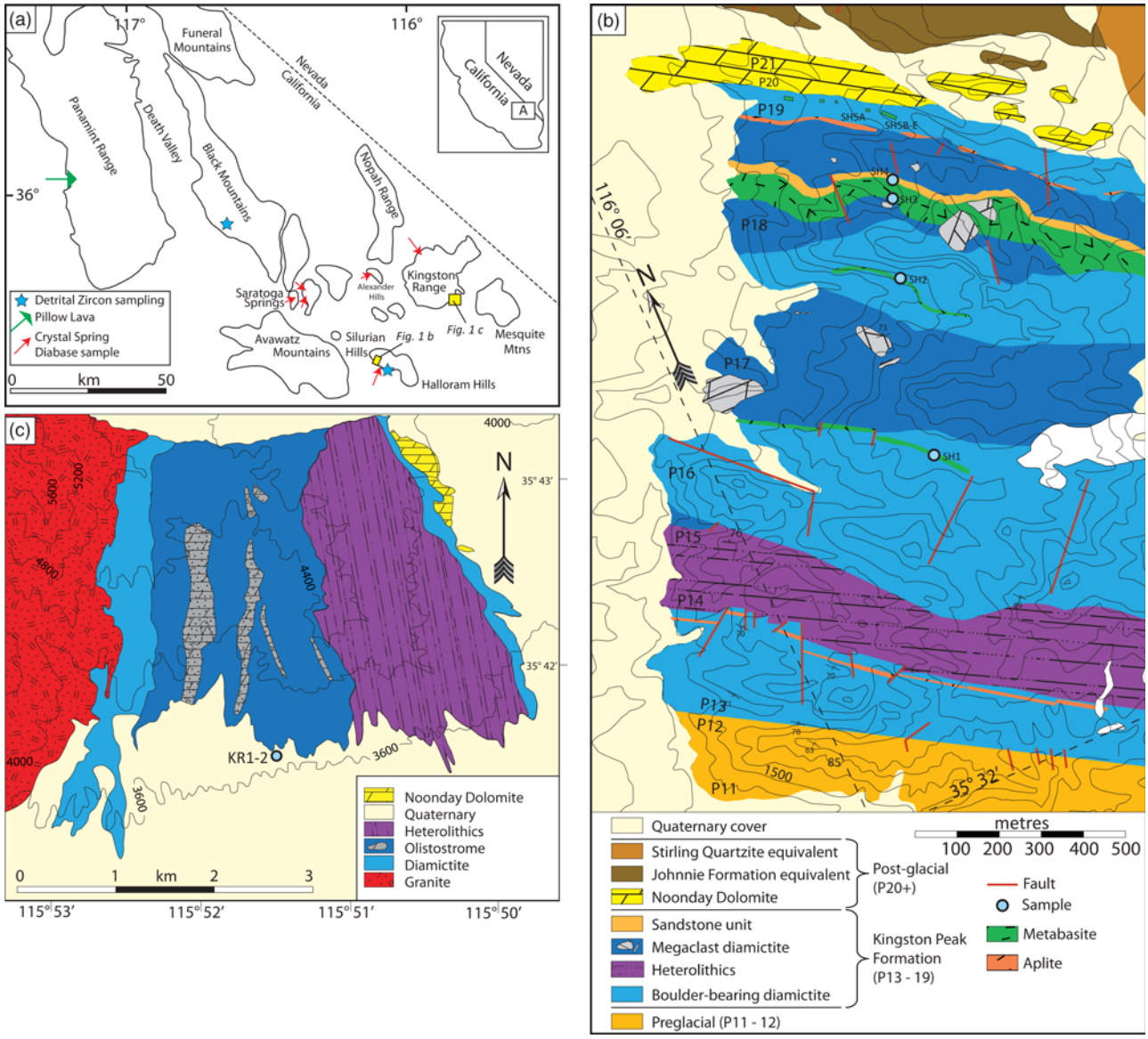

Fig. 1. Location maps of study area. (**a**) Regional sketch map with location of the Death Valley outcrop belts. Locations of (**b**) and (**c**) and samples of this study are indicated. (**b**) Geological sketch map of the western Silurian Hills region with sampled metabasite bodies shown (modified from Le Heron *et al.* 2017). P11–21 are mapping units of Kupfer (1960). (**c**) Geological sketch map of the southern Kingston Range indicating sample locality (modified from Busfield & Le Heron 2015).

Regionally pervasive metabasite intrusions, collectively named the Crystal Spring Diabase (CSD), occur within and below the Crystal Spring Formation (Hammond 1983, 1986). Two CSD ages are published, 1069 ± 3 Ma and 1087 ± 3 Ma (U–Pb baddeleyite; Heaman & Grotzinger 1992), but the latter is preferred as it is less discordant (Bright *et al.* 2014). Evidence that the CSD was intruded into wet, unconsolidated sediment strongly suggests that it was penecontemporaneous with deposition of the youngest Crystal Spring Formation, the Chert Member (Hammond 1983, pp. 32–40, 1986). The CSD is the western extremity of the recently defined Southwestern Laurentia Large Igneous Province (SWLLIP, *c.* 1080–1094 Ma; Bright *et al.* 2014). The Texas Panhandle (Li *et al.* 2007) is the province's eastern extremity. Owing to age uncertainties, the Cardenas basalt flows (Grand Canyon; Hendricks & Lucchitta 1974; Larson *et al.* 1994), Pecos mafic complex (New Mexico–Texas; Kargi & Barnes 1995) and mafic intrusions within the Pikes Peak batholith (Colorado; Smith *et al.* 1999) are only tentatively assigned to the SWLLIP.

In ascending order, the Horse Thief Springs (HTS) Formation, Beck Spring Dolomite and unit KP1, of the KPu, constitute one relatively conformable unit (Mrofka 2010; Mahon *et al.* 2014*b*; Smith *et al.* 2016). The basal HTS has a maximum age of 787 ± 11 Ma (U–Pb detrital zircon; Mahon *et al.* 2014*b*). It contains reworked fragments of the CSD and is separated from the underlying Crystal Spring Formation by a regionally pervasive unconformity, representing ≥300 myr (Maud 1979, 1983; Mahon *et al.* 2014*b*). Detrital zircon spectra from above and below this unconformity are distinctly different (Mahon *et al.* 2014*a*). However, whereas over 30 samples from multiple localities have been reported from above the unconformity, only three are reported from below it and all from the Kingston Range (Vogel 2004; MacLean 2007; MacLean *et al.* 2009; Mahon *et al.* 2014*a*,*b*; Smith *et al.* 2016). Detrital zircon sample F04-DV-14 (also labelled K04-DV-14) of Mulder *et al.* (2017) purports to be middle Crystal Spring Formation. However, no stratigraphic context is provided and its reported location (35.911535, −110.644025) is >450 km from the nearest known Crystal Spring Formation outcrop (Mulder *et al.*

2017, supplementary file 1). Therefore, as we are unable to verify the stratigraphic context of this sample, it is omitted from this study. The Beck Spring Dolomite is correlated between outcrops using micropalaeontology and the $\delta^{13}C$ 'Islay' anomaly (Smith *et al.* 2016). It is intruded by metabasites in the Panamint Range, unrelated to the CSD (Albee *et al.* 1981; Hammond 1983). Intermediate composition meta-igneous boulders (supplementary material) have been observed by the authors in low-grade marbles, a few metres beneath the KPu of the Silurian Hills (Fig. 2a) (Unit P12 of Kupfer 1960).

The Kingston Peak Formation (excluding KP1) unconformably overlies the Beck Spring Dolomite (or KP1). It is assigned to the Cryogenian on account of glacial characteristics (e.g. Hazzard 1939; Le Heron *et al.* 2014). In this paper it is referred to as simply Kingston Peak undifferentiated (KPu), owing to the lack of marker units and age control in the areas studied. Metabasite pillow lavas occur only at the KPu western extremity, in the Surprise member of the Panamint Range (Fig. 1) (Albee *et al.* 1981; Hammond 1983; Miller 1985). Hammond reported major elements from two such pillow lavas, although amphibolite-facies metamorphism probably mobilized these, along with selected rare earth elements for one pillow lava. These limited data were used to suggest that the pillow lavas are unrelated to the CSD (Hammond 1983, pp. 155–163). Outside the Panamint Range, metabasite sills are reported at the southeastern extremity of the KPu, in the Silurian Hills (Fig. 1). Some of these are thought to have been intruded concurrently with KPu deposition, suggesting a Cryogenian age (Kupfer 1960; Basse 1978). Stratigraphic correlations between the KPu of the Panamint Range and elsewhere, such as the Silurian Hills and Kingston range (Fig. 1), remain contested (Prave 1999; Macdonald *et al.* 2013). An Ediacaran cap carbonate, the Noonday Formation, locally unconformably or conformably overlies the KPu (Petterson *et al.* 2011; Creveling *et al.* 2016).

In the Silurian Hills, correlating the Pahrump Group has proven problematic (Maud 1979; Prave 1999; Mrofka 2010; Smith *et al.* 2016). The following summary uses the Silurian Hills mapping units of Kupfer (1960), in ascending stratigraphic order from P1 to P20 (Figs 1b and 2a). Units P1–4 are lithostratigraphically correlated to the lower Crystal Spring Formation members (Arkose to Dolomite members; Roberts 1974, 1976), including a CSD sill (Wright 1968; Hammond 1986). P5–12 are problematic, as petrographic study has found no microfossils (Shafer 1983), abundant $\delta^{13}C$ data have proven inconclusive (Prave 1999; Mrofka 2010; Smith *et al.* 2016) and lithostratigraphic correlations are tentative (Maud 1979). Detrital zircons from P7 and P11 exhibit the post-unconformity age spectra outlined above (Smith *et al.* 2016). However, this remains unproven as a correlation tool. P13–19 are clearly glacial and are attributed to the KPu (Basse 1978; Shapiro *et al.* 2014; Le Heron *et al.* 2017). Le Heron *et al.* (2017) interpreted two types of diamictite in the Silurian Hills: (1) boulder-bearing diamictite, transported by glacial action and characterized by rounded basement clasts; (2) megaclast-bearing diamictite, transported by slope failure and characterized by angular and disaggregated carbonate clasts, including olistoliths (Fig. 2a). P20 is the Noonday Formation (Prave 1999; Petterson *et al.* 2011; Fig. 6b). Within these KPu strata, Kupfer (1960, p. 199) described amphibolitized metabasite sills in P17. He argued that these were injected into shallow wet sediments during the deposition of upper P17 and lower P18, possibly with some subaqueous extrusion. Within the overlying P18, Kupfer noted sedimentary fragments of metabasite of the same description. Basse (1978, p. 72) additionally logged several sills within P18 and implied that some were contemporaneous with KPu sedimentation (Basse 1978, p. 53).

Methods

To investigate the stratigraphic context, age and source of the metabasite bodies in the KPu of the Silurian Hills, we present the following.

(1) Whole-rock geochemistry, field observations, U–Pb apatite and igneous zircon ages from KPu metabasite bodies of the Silurian Hills (samples SH1 to -5) (Table 1). This sampling targeted the logged 'sills' of Kupfer (1960, p. 191) and particularly Basse (1978, p. 72), within P17 and P18, along with a previously unpublished metabasite body in P19 (Table 1). By way of comparison we present a similar dataset, except without zircons, from a recognized metabasite olistolith (Calzia *et al.* 2000) in the Kingston Range (samples KR1, KR2).
(2) Whole-rock geochemistry of six *in situ* CSD intrusions, from various localities, as a potential source of the KPu metabasite bodies (samples CSD1 to -6) (Table 1).
(3) Whole-rock geochemistry and field observations of a pillow lava (sample HC1) from the KPu of the Panamint Range (Table 1), as a comparison with the Silurian Hills KPu metabasite bodies.
(4) U–Pb detrital zircon ages from the Crystal Spring Formation of the Silurian Hills (samples DZ-SH1 and -2) and Black Mountains (sample DZ-BM1), along with the proposed Horse Thief Springs Formation of the Silurian Hills (sample DZ-SH3) (Table 1). These data test whether characteristic detrital zircon spectra, from above and below the Crystal Spring unconformity, are consistently distinguishable in multiple Death Valley localities. If so, these spectra may be used to constrain the stratigraphy of the Silurian Hills and their metabasites.

In the Silurian Hills, metabasite bodies and the KPu were studied and described in detail during three field campaigns from 2015 to 2017 (Fig. 2a) (see also Le Heron *et al.* 2017). Likewise, 2014 and 2015 field campaigns placed the southern Kingston Range metabasite olistoliths (Calzia *et al.* 2000) into context (Fig. 2b) (see also Le Heron *et al.* 2018). In all samples, a number indicates relative stratigraphic level, whereas a suffix letter indicates along-strike duplication.

The Kingston Range olistolith (KR1) and one Silurian Hills metabasite body (SH3B) were selected for U–Pb dating by laser ablation inductively coupled plasma mass spectrometry (LA-ICP-MS). This was on the basis of abundant, well-preserved apatite in thin section. Five samples from the uppermost Silurian Hills metabasite (SH5) were also selected, despite apatite being less fresh and abundant. All mineral separation used standard techniques (i.e. jaw crushing, water table, heavy liquids and magnetic separation). All separated metabasite samples yielded apatite; SH5A-E additionally yielded zircons.

LA-ICP-MS was performed at Trinity College Dublin for all apatites, along with zircons of DZ-SH1, DZ-SH2 and SH5A - E. LA-ICP-MS was performed at the Arizona Geochronology Center for zircons of DZ-SH3, DZ-BM1 and aliquots of SH5B and C. Full details of LA-ICP-MS methods and standards are in the supplementary material.

Whole-rock geochemistry was mostly obtained by X-ray fluorescence (XRF). Major elements were determined at the University of Leicester and trace elements at Royal Holloway University of London (RHUL), with matrix corrections calculated from major element compositions. Additionally, two samples, SH5E and CSD5, were also analysed by inductively coupled plasma atomic emission spectrometry (ICP-AES) and ICP-MS at RHUL.

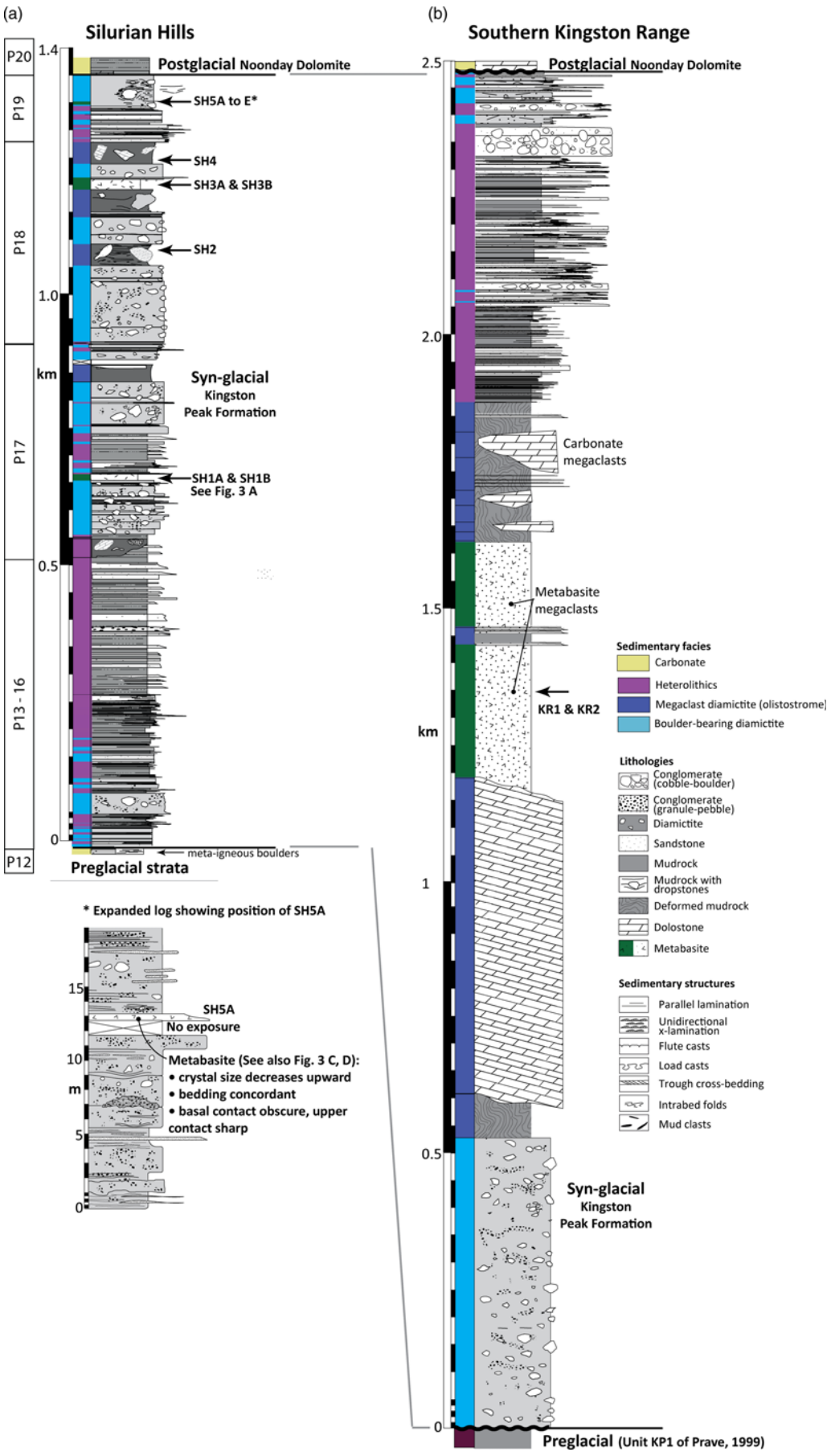

Fig. 2. Stratigraphic columns of the KPu, including sample locations, in both study areas. (**a**) Silurian Hills, simplified from Le Heron *et al*. (2017). Expanded log shows detail of a typical contact between metabasite and enclosing metasediments, in which the lower contact is not exposed. P12–20 are approximate mapping units of Kupfer (1960). Details of meta-igneous boulder in P12 are given in the supplementary material. (**b**) Southern Kingston Range adapted from Le Heron *et al*. (2018).

Table 1. *Samples of this study*

Sample	Coordinates	Description	Analysis
KR1	35° 41.436, −115° 51.452	KPu metabasite olistolith, Southern Kingston Range	X, A
KR2	35° 41.418, −115° 51.457	KPu metabasite olistolith, Southern Kingston Range (immature sedimentary rock)	X
SH1A	~35° 32.421, −116° 05.665	KPu metabasite body, Silurian Hills (P17). Targeted sill: 4900 ft/1495 m (Kupfer), 1500 m (Basse)	X
SH1B	~35° 32.421, −116° 05.665	KPu metabasite body, Silurian Hills (P17). Targeted sill: 4900 ft/1495 m (Kupfer), 1500 m (Basse)	X
SH2	35° 32.645, −116° 05.580	KPu metabasite body, Silurian Hills (P18). Targeted sill: 1875 m (Basse)	X
SH3A	35° 32.739, −116° 05.565	KPu metabasite body, Silurian Hills (P18). Targeted sill: 1950 m (Basse)	X
SH3B	35° 32.739, −116° 05.561	KPu metabasite body, Silurian Hills (P18). Targeted sill: 1950 m (Basse)	X, A
SH4	35° 32.767, −116° 05.556	KPu metabasite clast, near metabasite body (P18). Targeted sill: 2000 m (Basse)	X
SH5A	35° 32.874, −116° 05.541	KPu metabasite body, Silurian Hills (P19)	X, A, Z
SH5B	35° 32.859, −116° 05.515	KPu metabasite body, Silurian Hills (P19)	X, A, Z
SH5C	35° 32.859, −116° 05.515	KPu metabasite body, Silurian Hills (P19)	X, A, Z
SH5D	35° 32.865, −116° 05.518	KPu metabasite body, Silurian Hills (P19)	X, A, Z
SH5E	35° 32.859, −116° 05.515	KPu metabasite body, Silurian Hills (P19)	X, A, Z, I
CSD1	35° 43.099, −116° 21.777	CSD metabasite, Saddle Peak Hills	X
CSD2	35° 43.409, −116° 22.236	CSD metabasite, Saddle Peak Hills	X
CSD3	35° 42.731, −116° 24.156	CSD metabasite, Saratoga Spring talc mine	X
CSD4	35° 47.916, −115° 57.517	CSD metabasite, Kingston Range	X
CSD5	35° 31.702, −116° 06.232	CSD metabasite, Silurian Hills (P3)	X, I
CSD6	35° 46.827, −116° 07.566	CSD metabasite, Western Talc Mine	X
HC1	36° 04.290, −117° 10.091	KPu metabasite pillow lava, Panamint Range	X
DZ-SH1	35° 31.703, −116° 06.232	Granular conglomerate, Silurian Hills (P1). Crystal Spring Fm, basal conglomerate, 1.0 m above base of Pahrump Gp	DZ
DZ-BM1	35° 57.276, −116° 38.064	Granular conglomerate, Black Mountains. Crystal Spring Fm, basal conglomerate, 0.75 m above base of Pahrump Gp	DZ
DZ-SH2	35° 31.727, −116° 06.215	Granular conglomerate, Silurian Hills (P2). Crystal Spring Fm, Arkose member, *c*. 50 m above base of Pahrump Gp	DZ
DZ-SH3	35° 31.865, −116° 06.291	Orthoquartzite, Silurian Hills (P6). Horse Thief Springs Fm (?), *c*. 250 m above base of Pahrump Gp	DZ

KPu, Kingston Peak Formation; CSD, Crystal Spring Diabase; (P…), Silurian Hills mapping unit P… of Kupfer (1960); 'Targeted sill' indicates stratigraphic position, within the measured sections of Kupfer (1960, p. 191) or Basse (1978, p. 72), of the published 'sill' targeted by a given sample of this study. Analysis: X, whole-rock XRF; I, whole-rock ICP-MS and ICP-AES; A, U–Pb apatite; Z, U–Pb metabasite zircon; DZ, U–Pb detrital zircon.

Full details of whole-rock geochemistry methods and standards are in the supplementary material.

Field and petrographic data from metabasites of the Kingston Peak Formation and the Crystal Spring Diabase

Description

In the KPu of the Silurian Hills, samples SH1, -2, -3, -5 were taken from metabasite bodies occurring as tabular, bed-like units at multiple stratigraphic horizons, associated with the boulder and megaclast diamictite facies (Figs 1b and 2a, Table 1). Sample SH4 is from a 35 cm metabasite boulder of the boulder-bearing diamictite facies (Figs 1b, 2a and 3b). The bodies are concordant within steep, northward-dipping strata and are up to *c.* 10 m thick (Fig. 3a). Along-strike they typically become disaggregated, up to the limit of their exposure, where they often weather into boulder-like outcrops (Fig. 3e), which may include metabasite diamictite clasts (e.g. sample SH4, Fig. 3b). The lower margins of the metabasite bodies are not generally exposed, whereas the intermittently exposed upper margins are sharp (Fig. 3f). The lowermost and uppermost bodies, SH1 and SH5, exhibit fining of crystal size towards their contact with overlying metasedimentary units, from medium plagioclase laths to a microcrystalline fabric (Fig. 3d). In thin section, the Silurian Hills metabasites define two groups, broadly relating to marginally lower (SH2, -3, -4) and higher (SH1 and -5) metamorphic grades. SH3 is typical of the lower-grade group, with plagioclase and chlorite representing the rock-forming minerals and the dominant accessory minerals being biotite, calcite and apatite. SH5 exemplifies the higher-grade group, in which the rock-forming minerals are altered plagioclase and amphibole and the dominant accessory minerals are calcite and apatite. Despite this, clear primary igneous textures are preserved, including plagioclase laths and more equant millimetre-scale feldspars. Apatites are generally hexagonal, prismatic and euhedral, characteristic of a magmatic origin (Fig. 3c). No preferred mineral alignment was observed within the metabasites or the enclosing metasedimentary strata.

The uppermost metabasite body in the Silurian Hills (SH5) is exposed intermittently along-strike for 275 m, and varies in thickness from 0.8 to 2 m. However, one 11 m long segment is exceptional (Fig. 4). It consists of three thinner tabular bodies, each around 20 cm thick and 2 m long, that occur metres above (SH5C, -D) and decimetres below (SH5E) a thicker, more continuous metabasite body (SH5B) (Fig. 4a–d). One thinner body, SH5D, pinches out at one margin, suggesting a lenticular geometry. Both lower and upper margins of these bodies are well preserved. The thicker body is medium crystalline in the core, becoming microcrystalline towards its upper and lower margins, whereas the thinner bodies are microcrystalline throughout. The enclosing metasedimentary units are well bedded and often laminated. They lack significant soft-sediment deformation but contain dropstones (Fig. 4a, b, d and e) (Shapiro 2014; Le Heron *et al*. 2017). The metabasite bodies cross-cut these strata, within decimetres of the dropstones, except SH5E, which is bedding-concordant (Fig. 4). Forty metres along-strike from this exceptional exposure, SH5A exhibits typical characteristics of stratigraphically lower metabasite bodies. Its lower margin is not preserved, it is concordant with bedding and it weathers into boulder-like forms along-strike (Fig. 3e), although no diabase clasts were observed within those forms.

In the southern Kingston Range, metabasite olistoliths occur within the middle of the olistostrome outcrop of the KPu (Fig. 1 c) (Calzia *et al*. 2000). Those reported herein exceed 25 m in thickness and are separated by metasedimentary units (Fig. 2b). Each is highly irregular and fragmented within the stratigraphy into blocks, up to hundreds of metres wide (Fig. 5a). Internally, these metabasite

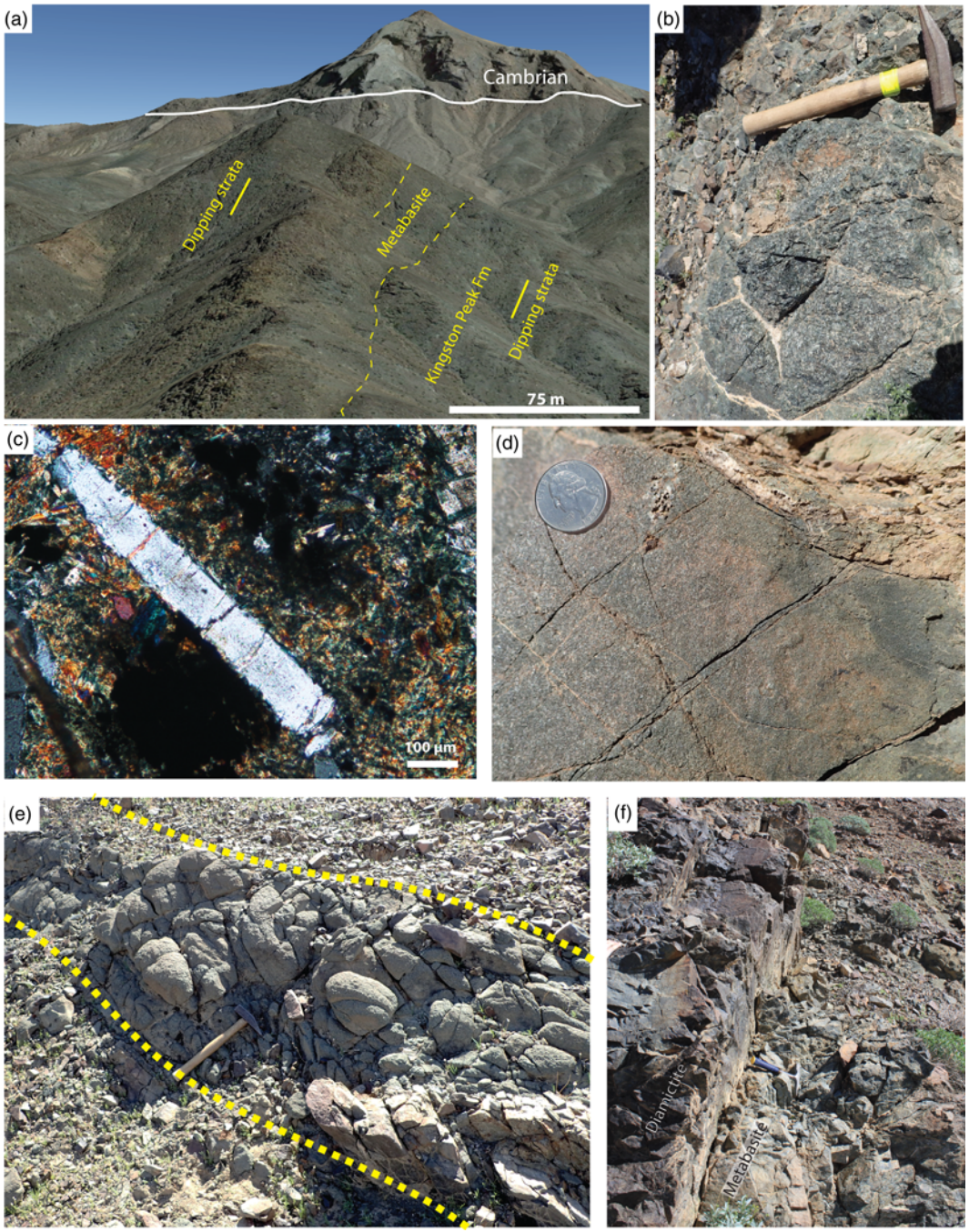

Fig. 3. Metabasite rocks in context, Silurian Hills. (**a**) Google Earth image (Landsat/Copernicus), looking eastward, of the lowermost metabasite body, SH1. (**b**) Disaggregated texture of metabasite in diamictite at its along-strike terminus, boulder sample SH4. (**c**) Thin section of SH3B showing euhedral apatite under crossed polars. (**d**) Diminishing crystal size, bottom left to top right, towards the margin of metabasite body SH1. (**e**) Metabasite body SH5 weathering into rounded boulder-like forms, 250 m west of the exceptional 11 m exposure. Dashed lines indicate approximate strike of metabasite body. (**f**) Sharp upper contact at base of hammer, between metabasite body (SH1) and overlying diamictite.

olistoliths consist of lens-like forms (phacoids) (Fig. 5b–d), which in some cases could be mistaken for xenoliths (Fig. 5c). They show a transition from coherent rock masses to disaggregated material along-strike and the upper contact of one olistolith shows a sharp, yet concordant, contact with overlying graded sandstones and conglomerates (Fig. 5d). The conglomerates (Fig. 5e) contain a variety of lithic fragments including quartzite and carbonate, but significantly include cobbles and boulders of metabasite, sometimes set within a highly comminuted metabasite matrix (sample KR2; Fig. 5f). There is therefore a continuum of lithologies, from coherent but phacoidal metabasite body, through mafic sedimentary breccia, to metabasite–quartzite–carbonate conglomerate. In thin section, the KR1 mineral assemblage is similar to the lower-grade metabasite group described from the Silurian Hills. Sample KR2 is from the comminuted metabasite matrix and is therefore a highly immature sedimentary rock, albeit of largely mafic material (Fig. 5f).

From the Kingston Peak Formation in the Panamint Range, HC1 is a finely crystalline metabasite with a sporadically developed weak lineation (Fig. 6a). It forms a unit at least 10 m thick, concordant with enclosing diamictites of the Surprise Member. Internally, this metabasite consists of rounded decimetre-scale clast-like or pillow-like forms (Fig. 6a), with similarities to forms associated with metabasites in the Silurian Hills and Kingston Range (Figs 3e, 5c, e and 6b). However, these forms are not accompanied by non-metabasite material.

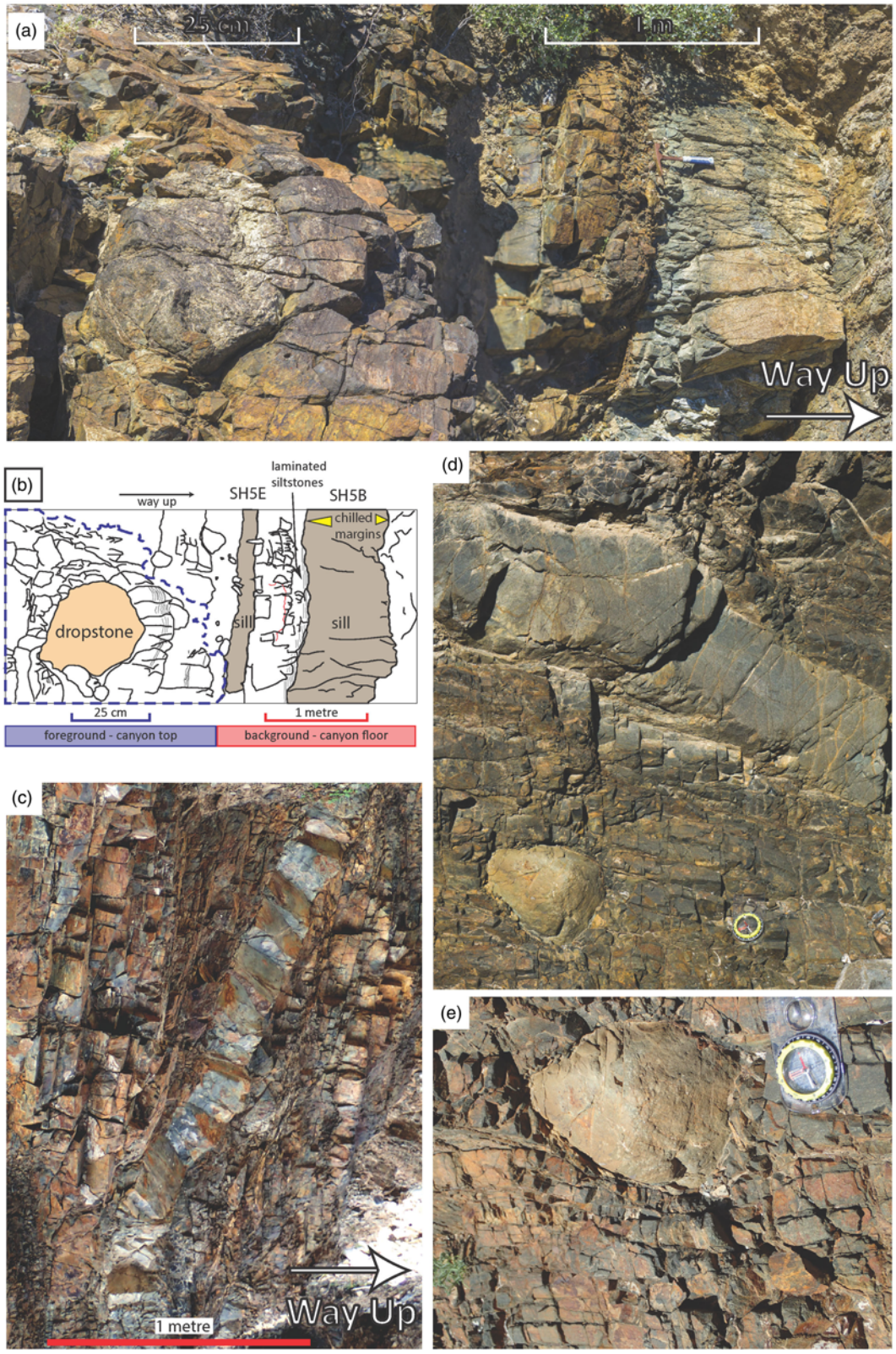

Fig. 4. Metabasite SH5 intruding dropstone-bearing strata. (**a**) Dropstone beneath intrusions SH5B and E. Collage of multiple images, courtesy of C. Zalunardo. The sill is in a steep-sided canyon, *c.* 5 m deep, foreshortening the left of the image. (**b**) Annotated sketch of (**a**). (**c**) SH5C dyke sharply cutting through well-bedded country rock. (**d**) SH5D cross-cutting laminated sediments at a low angle, with 21 cm dropstone below. (**e**) Detail of 21 cm dropstone showing deflection and truncation of laminae.

From the CSD, samples from the Silurian Hills (CSD5) and Alexander Hills (CSD6) were examined in thin section. Both have a mineral assemblage similar to the higher metamorphic grade group described from the KPu metabasite bodies of the Silurian Hills.

Interpretation

Reappraisal of the Silurian Hills succession, previously mapped and/or logged by several researchers (Kupfer 1960; Basse 1978; Shapiro *et al.* 2014; Le Heron *et al.* 2017), affirms that the

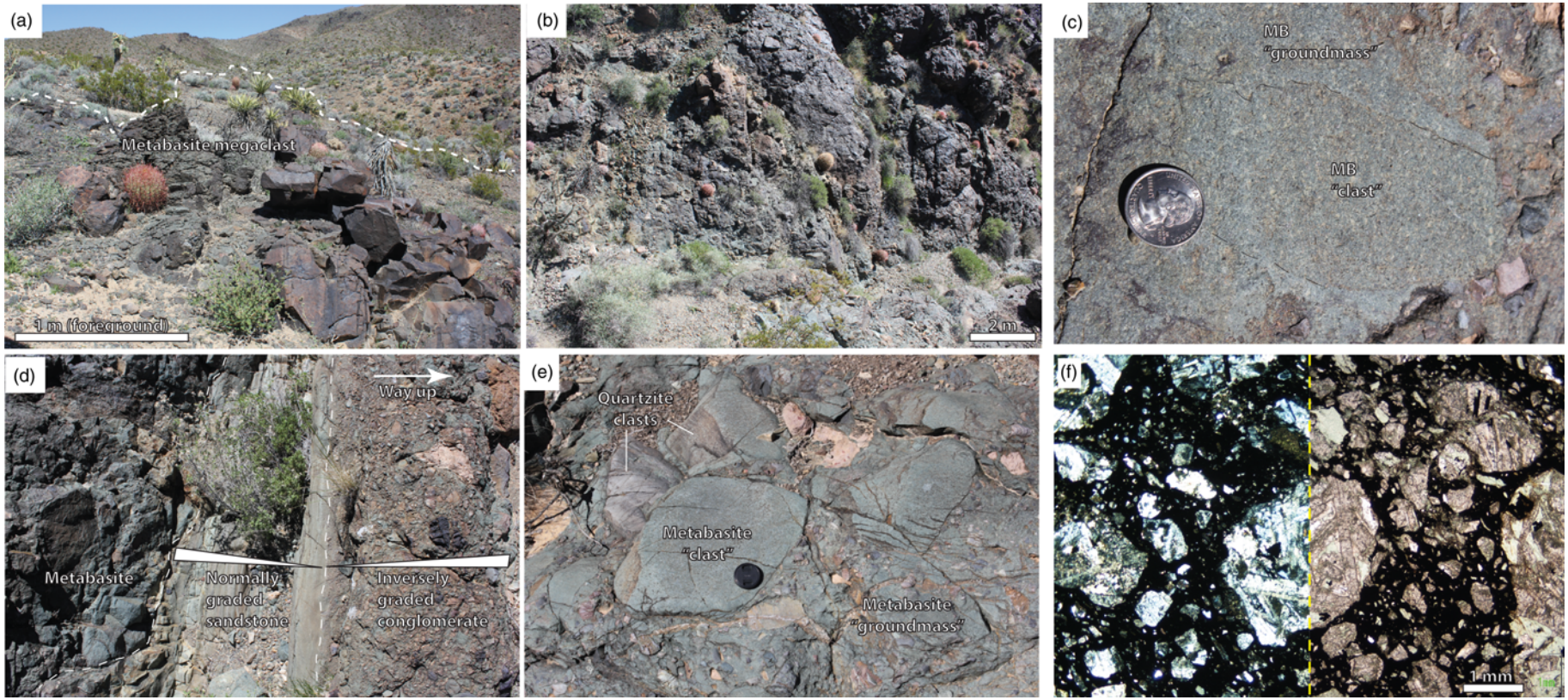

Fig. 5. Metabasite rocks in context, southern Kingston Range. (**a**) 15 m wide outcrop of a 100 m long metabasite olistolith, with approximately bedding-parallel upper and lower contacts (note disaggregated character). (**b**) Basal surface of the 100 m olistolith (note boulder-sized phacoids). (**c**) 'Clast' of metabasite within a groundmass of similar composition. (**d**) Contact between metabasite olistolith and overlying graded beds. (**e**) Graded conglomerate just above the olistolith in (**d**); both metabasite and non-igneous clasts. (**f**) Thin section of KR2. Left: crossed-polars. Right: plane-polarized light. (**c**)–(**e**) are adapted from Le Heron *et al.* (2018).

metabasite bodies, except SH5B–E, show bedding-concordant relationships, justifying their previous interpretation as sills. Indeed, diminishing crystal size towards the margin of the metabasite body supports a chilled margin interpretation. Additionally, the tendency of the metabasite bodies to crop out at or near lithological boundaries (Fig. 1b) might suggest intrusive exploitation of lithological contrasts. In spite of this, one observation allows for an alternative explanation, namely the along-strike transition of the metabasite bodies from coherent to disaggregated or brecciated material. This disaggregated appearance is consistent with the metabasite bodies having been transported downslope and incorporated into the KPu as olistoliths. The long-recorded presence of metabasite clasts in the KPu of the Silurian Hills (Kupfer 1960; Basse 1978) is consistent with this interpretation. The uppermost metabasite body, SH5, on the other hand clearly indicates an intrusion *in situ* with its country rock, at least for an 11 m segment. Cross-cutting of delicately laminated siltstones, without soft sediment deformation or brecciation, is inconsistent with gravitational emplacement of a metabasite body into soft or consolidated sediments. The depositional age of the closely surrounding dropstones must therefore be greater than the magmatic age of SH5.

The metabasite bodies of the Silurian Hills are comparable with the metabasite olistoliths of the Kingston Range, previously mapped by Calzia *et al*. (2000). Most notable is the tendency to disaggregate along-strike into sedimentary fragments. Olistoliths are associated with the emplacement of unsorted material (e.g. Robertson 1977), yet a striking similarity between the upper contacts of the Kingston Range metabasite olistoliths and a typical Silurian Hills metabasite body is that both are overlain by well-organized (graded) deposits (Fig. 2, see inset to a). Is it therefore possible that the metabasite bodies of the Silurian Hills were once sills, but have been remobilized and redeposited largely intact and have therefore maintained stratigraphic relationships diagnostic of an *in situ* sill?

Fig. 6. Comparison of rounded metabasite forms. (**a**) Sampled pillow lava (HC1) from the KPu in the Panamint Range. (**b**) Conglomerate/diamictite from the KPu of the Southern Kingston Range, tens of metres from sampled metabasite olistolith KR1. Carbonate boulder, right of image. Metabasite clast, above hammer. Compare to Fig. 3b and e (Silurian Hills), and Fig 5c and e (Kingston Range).

The Panamint Range pillow lava sample, HC1, was taken from a unit mapped as 'pillow basalt and amphibolite' by Albee *et al*. (1981). Its rounded forms are consistent with pillow lavas, as is its concordance within the enveloping sedimentary rocks. These features are, however, also comparable with features of the Silurian Hills and Kingston Range metabasites. Moreover, Miller (1983) reported these mapped pillow lavas locally forming pillow breccias (*sensu* Carlisle 1963), which could be compared with the along-strike disaggregation and brecciation of the Silurian Hills and Kingston Range metabasites. The pillow lavas are, however, well established elsewhere as being *in situ* within the stratigraphy (e.g. Miller 1985) and that interpretation is not challenged here. Instead, emphasis is placed upon the similarities in diagnostic field observations between the clearly transported Kingston Range olistolith, the clearly *in situ* pillow lavas and the contentious metabasite bodies of the Silurian Hills. It appears that distinguishing between sill and olistolith, using field observation alone, may be problematic in certain instances.

The Crystal Spring Diabase (CSD) is the proposed source of the sampled Kingston Range olistolith (Calzia *et al*. 2000). From over 40 CSD samples, Hammond (1983, p. 59) observed two mineral assemblage end members, likened to greenschist and amphibolite facies. Neither had a preferred mineral alignment. The two CSD samples petrographically examined herein, CSD5 and CSD6, closely resemble Hammond's amphibolite end member. Likewise, the higher metamorphic grade group of the Silurian Hills KPu (SH1 and SH5) also resembles Hammond's amphibolite end member, whereas the lower grade group (SH2–4) and Kingston Range olistolith (KR1) resemble Hammond's greenschist end member. Hammond noted that the mineral assemblage end member of the CSD tends to be consistent for a given locality. Thus, if we posit that metamorphism of the CSD predated the Cryogenian transport of olistoliths, then mixing of the two end members, within the Silurian Hills metabasites, might suggest olistoliths transported in from multiple CSD localities.

Although these features are consistent with a link between the Silurian Hills metabasite bodies and the CSD, they could equally be features applicable to other metabasites, unrelated to the CSD. Therefore to test this proposed link further, geochemical comparison are required, especially of immobile trace elements.

Geochemical data from metabasites of the Kingston Peak Formation and the Crystal Spring Diabase

Description

Major elements of the KPu metabasites (Tables 2 and 3), in the Silurian Hills and Kingston Range, display no clear systematic behaviour of SiO_2, Al_2O_3, CaO, NaO and K_2O (note that KR2 is an immature sedimentary rock and not considered in this geochemistry section). By contrast, TiO_2 correlates positively with P_2O_5 and negatively with Mg# (Fig. 7). It is bimodally distributed between a low-Ti (KR1, SH1, SH5) and a high-Ti group (SH2, SH3, SH4). The latter also has higher MnO. Relative to the CSD, and other KPu metabasite bodies, SH1B is TiO_2 depleted but highly MgO enriched (24.8 wt%). CSD major elements of this study, and those previously published (Hammond 1983), show the same systematic behaviours as described above for the KPu (Fig. 7). Unlike the KPu, however,

all CSD samples are TiO_2 enriched. Nevertheless, the KPu low-Ti group plots on the same TiO_2 v. Mg# and P_2O_5 trendlines as the CSD (Fig. 7).

The CSD and KPu trace elements, excluding the Panamint Range, produce similar plots on multi-element diagrams (Figs 8 and 9). These diagrams are populated with typically immobile elements, along with Ba and Sr. Within both the CSD and KPu, a 'depleted' (CSD3, -5, -6; SH1, -5) and an 'enriched' (CSD1, -2, -4; SH2, -3, -4) trace element group are recognized. Relative to the enriched group, the depleted group has a flatter Th–Nb–La profile and is depleted in most plotted elements (dashed line in Fig. 8). The Kingston Range olistolith, KR1, is intermediate between these two groups and, in common with SH1 and SH5 of the depleted group, lacks a positive Ti-anomaly. Within the dropstone-associated metabasite body, SH5, all samples produce near-identical multi-element plots (inset to Fig. 9a). Furthermore, multi-element plots, using an extended range of elements determined by ICP-MS and ICP-AES, demonstrate remarkable similarity between this metabasite body and the CSD from the Silurian Hills (CSD5; Fig. 9a). Conversely, the Panamint Pillow lava (HC1) plots distinctly differently from all other samples of this study, exhibiting light REE depletion and a positive Nb anomaly (Fig. 9b).

Selected trace element ratios of the CSD and KPu metabasites, excluding the Panamint Range, plot similarly to published SWLLIP mafic intrusions from Arizona and New Mexico (Fig. 10a and b). In La/Ba v. La/Nb space, the KPu and CSD form a single group defining a positive correlation (Fig. 10c). By contrast, in Th/Yb v. Nb/Yb and Th/Y v. Nb/Y space, they separate into the enriched and depleted trace element groups noted in Figure 8, both forming positive correlations (Fig. 10d). The scatter of these CSD and KPu ratios is comparable with that for other published large igneous province (LIP) data (Fig. 10c and d).

Interpretation

The similarities of Nb, La, Ce, P, Nd, Zr, Hf and Y in the multi-element diagrams (Figs 8 and 9), along with the clustering and/or correlation on elemental ratio plots (Fig. 10), suggest that the CSD and KPu metabasites, excluding the Panamint Range, are comagmatic. By contrast, owing to multi-element diagram differences (Fig. 9b), the Panamint Range pillow lava (HC1) is unlikely to be related to the CSD or KPu metabasites.

Major element data are often unreliable in such ancient metamorphosed rocks and metasomatism probably mobilized the major elements that lack systematic behaviour. Nevertheless, P_2O_5, TiO_2 and Mg# correlations suggest that fractional crystallization played a role in major element diversity, within a broadly basaltic suite (e.g. DePaolo 1981) (Fig. 7, Table 2). Despite TiO_2 depletion, relative to the CSD, the low-Ti KPu group is within the TiO_2 range of the SWLLIP (e.g. Li *et al*. 2007; Bright *et al*. 2014) and lies on the Mg# and P_2O_5 trendlines of the CSD (Fig. 7). Therefore, in conjunction with the similarities to the CSD outlined above (Figs 7–10), the suggestion that the CSD and the low-Ti KPu group are comagmatic remains reasonable.

The MgO of SH1B (24.8 wt%), from the lowermost Silurian Hills metabasite body, is enriched not only above the other samples of this study (maximum 9.0 wt%), but also above 185 MgO values from across the SWLLIP, reviewed for this study (MgO <12 wt%; Fouts 1974; Hendricks & Lucchitta 1974; Hammond 1983, 1990; Larson *et al*. 1994; Smith *et al*. 1999; Li *et al*. 2007; Bright *et al*. 2014). This may partly be metasomatic, associated with high loss on ignition (LOI; 4.83 wt%). SH1B is, however, interpreted as a less evolved member, possibly an olivine cumulate, of the CSD–KPu comagmatic suite. First, it lies on the same fractionation related trendline, but with a much higher Mg# than other samples (Fig. 7). Second, relative to other samples, it is enriched in compatible elements Ni (821 ppm) and Cr (1693 ppm) and depleted in incompatible elements, yet has a similar multi-element diagram pattern (Table 2, Fig. 8).

Multi-element diagrams (Figs 8 and 9) indicate that the CSD and KPu samples of this study have a subduction-like geochemistry; for example, a negative Nb anomaly. As noted by Bright *et al*. (2014), such signatures are common within continental LIPs and bear witness to contamination by crust, or interaction with subduction-modified lithosphere. Slab break-off beneath the region, in association with the Grenville Orogeny, could have contributed to this anomaly (Bright *et al*. 2014; Mulder *et al*. 2017).

Hammond interpreted the CSD as mildly alkaline, based upon major elements and 'modest enrichment' of rare earth elements (1986, p. 314). However, major element mobility, under metamorphic conditions, renders this interpretation problematic. By contrast, the trace element discrimination method of Winchester & Floyd (1976, fig. 11), used in Figure 10a, is relatively robust to metamorphic processes (Smith & Smith 1976) and the only major element it uses, P_2O_5, is immobile in our samples (Fig. 7). Figure 10a strongly suggests that all CSD and KPu of this study are mildly tholeiitic and that other SWLLIP samples, from Arizona and New Mexico, are likewise tholeiitic to transitional (Fig. 10a). Therefore the CSD and SWLLIP were probably more extensional in character than the 'limited rifting' suggested by Hammond (1990). Furthermore, as CSD emplacement was penecontemporaneous with deposition of the youngest Crystal Spring Formation, these sediments may also have been deposited in an extensional setting, such as a rift rather than foreland basin (see Mulder *et al*. 2017). Additionally, Figure 10a suggests that the Panamint pillow lava (HC1) is tholeiitic. This strengthens the previous tholeiite suggestion of Hammond (1983, p. 158), which was based on very limited immobile element data, but has often been cited as evidence of an extensional setting during KPu deposition (e.g. Miller 1985; Prave 1999; Mahon *et al*. 2014*a*).

Hammond (1990, fig. 8) defined two SWLLIP trace element ratio groups, suggested to represent different parental magmas, and noted the CSD in or near Group B only. The CSD and KPu of this study likewise plot in or near Group B (Fig. 10b), as do SWLLIP mafic intrusions, from Arizona and New Mexico, that were published since Hammond's paper. These findings support the KPu metabasite bodies belonging to the CSD and SWLLIP.

The positive correlation of La/Ba v. La/Nb, for the CSD–KPu comagmatic suite (Fig. 10c), suggests an ocean island basalt (OIB) and/or asthenospheric mantle source influence (Jourdan *et al*. 2009). This interpretation relies upon samples being relatively free of crustal contamination, which Hammond (1986, 1990) argued is the case for the CSD. However, countering this, the enrichment of samples above the mid-ocean ridge basalt MORB–OIB defined line in Th/Yb v. Nb/Yb space (Fig. 10d) suggests crustal contamination (Pearce 2008). The separation into two positively correlating groups, in both Th/Yb v. Nb/Yb and Th/Y v. Nb/Y space, supports the idea that the depleted and enriched trace element groups (Fig. 8) are genetically related subgroups, spanning a comagmatic suite of CSD and KPu metabasites (Fig. 10d).

U–Pb apatite and zircon geochronology from the metabasites of the Kingston Peak Formation and Crystal Spring Diabase

U–Pb dating of apatite is more challenging than U–Pb zircon dating, as apatite typically yields lower U and Pb concentrations and higher common Pb to radiogenic Pb ratios. This nearly always necessitates common Pb correction. Unlike zircon, which is generally restricted to igneous rocks of felsic composition, apatite is a nearly ubiquitous accessory phase in igneous rocks of both felsic and mafic

Table 2. *Whole-rock chemistry determined by X-ray fluorescence*

	SH1A	SH1B	SH2	SH3A	SH3B	SH4	SH5A	SH5B	SH5C	SH5D	SH5E	KR1	KR2	CSD1	CSD2	CSD3	CSD4	CSD5	CSD6	HC1	2σ
Major oxides (wt%)																					
SiO_2	49.73	46.39	44.11	48.59	51.43	44.74	50.23	49.13	47.87	48.63	49.74	52.85	51.11	48.75	47.15	47.45	46.50	49.31	46.77	53.62	0.92
TiO_2	1.46	0.70	3.45	3.31	3.24	3.65	1.26	1.23	1.32	1.33	1.31	1.62	2.94	4.23	5.22	2.48	3.37	3.19	2.83	0.59	0.02
Al_2O_3	16.0	9.1	16.5	13.0	12.9	14.6	15.0	16.2	16.7	17.2	16.8	13.6	15.3	13.3	11.8	17.7	15.0	14.4	16.6	14.0	0.39
Fe_2O_3	10.50	12.45	11.71	19.30	16.02	13.87	9.91	10.36	10.71	9.97	9.58	11.35	15.37	16.95	17.63	12.04	17.04	13.11	13.60	12.15	0.08
MnO	0.145	0.155	0.304	0.208	0.224	0.229	0.162	0.176	0.157	0.150	0.215	0.169	0.090	0.233	0.229	0.181	0.209	0.247	0.156	0.187	0.003
MgO	8.6	24.7	4.7	3.7	5.5	6.1	8.4	7.8	9.0	8.7	7.9	7.3	8.4	4.8	4.8	6.7	5.3	6.5	6.8	7.0	0.09
CaO	7.5	4.8	13.4	7.1	6.1	12.0	10.4	10.2	9.7	9.0	8.6	8.6	1.9	5.8	8.4	8.4	7.2	8.0	7.9	6.9	0.09
Na_2O	3.3	0.8	3.0	3.1	3.1	2.9	3.0	2.8	2.5	2.7	3.0	2.0	3.1	2.3	2.4	3.0	2.9	3.6	2.8	5.0	0.12
K_2O	2.04	0.22	1.73	0.43	0.67	1.17	1.01	1.52	1.36	1.69	2.09	1.95	0.95	2.56	1.48	1.50	1.62	0.96	1.82	0.27	0.02
P_2O_5	0.28	0.19	0.68	0.91	0.51	0.40	0.25	0.26	0.33	0.34	0.34	0.34	0.45	0.61	0.45	0.31	0.47	0.35	0.39	0.05	0.01
Trace sum	0.38	0.50	0.40	0.35	0.33	0.38	0.38	0.40	0.39	0.40	0.38	0.29	0.33	0.42	0.39	0.30	0.40	0.34	0.28	0.24	–
Total (*N*)	100.0	100.0	100.0	100.0	100.0	100.0	100.0	100.0	100.0	100.0	100.0	100.0	100.0	100.0	100.0	100.0	100.0	100.0	100.0	100.0	–
Total (*M*)	99.15	99.71	98.51	99.36	99.36	99.44	99.64	98.97	99.43	99.76	99.13	99.22	100.32	99.58	99.13	100.63	99.23	98.58	99.88	99.26	–
LOI	1.66	4.83	5.83	1.06	0.84	3.05	1.92	2.84	1.18	1.74	2.10	9.73	5.30	1.81	1.00	2.47	2.44	1.13	2.69	1.32	–
Trace elements (ppm)																					
Ni	117.7	864.9	153.5	20.2	26.5	41.5	83.4	60.5	170.6	162.6	120.9	125.8	73.5	28.9	35.6	121.7	107.8	56.6	82.6	91.8	2.9
Co	34.7	91.7	73.3	77.7	61.6	39.1	40.8	29.4	39.8	39.5	37.4	44.1	29.5	53.4	48.8	48.6	57.6	45.7	56.2	50.8	1.4
Cr	314.3	1784.1	253.0	<5	65.2	67.7	601.5	671.9	431.2	435.8	405.2	137.3	115.3	<5	5.5	176.1	152.8	154.0	50.7	136.1	5
V	268.9	142.3	410.0	398.6	436.6	698.5	318.9	324.5	275.2	270.2	272.9	243.5	282.3	342.1	457.5	227.1	410.7	389.1	219.6	359.7	2.4
Sc	35.8	16.8	42.6	47.1	50.6	72.9	51.4	58.0	34.7	35.9	36.6	23.6	35.7	40.6	50.0	29.1	40.0	51.5	28.9	54.9	0.9
Cu	23.4	36.3	34.3	163.4	209.7	6.2	17.5	25.8	4.8	6.6	22.5	55.9	65.6	157.0	220.7	61.0	214.7	94.9	35.3	117.2	0.5
Zn	62.7	82.5	108.5	97.2	123.1	120.4	76.6	89.5	87.7	99.4	69.6	171.2	172.2	192.6	154.6	109.9	141.3	147.4	94.2	75.3	0.6
As	1.2	9.1	1.0	1.7	0.8	1.3	1.0	2.3	0.4	3.5	4.2	3.1	1.5	4.0	1.4	0.8	13.0	1.7	4.3	1.8	0.3
S	136	30	91	189	306	25	105	141	178	457	125	60	151	476	902	427	152	391	522	114	1.7
F	504	108	599	656	525	649	320	404	526	606	449	540	968	804	484	343	473	371	420	143	16
Cl	430	218	255	377	348	274	351	422	427	393	307	172	124	337	570	286	264	199	236	211	10.7
Br	0.4	0.2	0.3	0.5	0.5	0.3	0.2	0.7	0.3	0.6	0.4	0.7	0.3	2.8	1.4	0.6	1.1	0.5	0.9	0.6	0.1
Ga	17.0	11.1	22.3	23.7	20.7	23.4	17.5	17.4	18.5	17.8	16.8	17.2	20.6	25.1	23.2	18.1	24.8	18.8	18.6	11.0	0.7
Pb	3.2	1.0	12.9	10.8	9.0	12.3	12.1	7.8	13.3	17.1	9.7	7.9	8.9	18.6	15.9	9.0	7.7	8.4	3.9	4.5	0.2
Sr	531	137	303	375	225	342	469	477	493	535	532	171	102	223	253	443	390	503	486	208	1.7
Rb	82.1	2.9	68.2	16.0	21.3	45.0	29.4	58.5	39.7	62.0	75.3	44.3	35.9	81.6	40.4	48.2	38.5	28.7	50.3	10.2	0.2
Ba	517	61	563	363	344	416	456	326	412	358	448	418	475	713	458	239	526	297	289	336	5.6
Zr	133.5	81.2	179.9	182.5	154.3	149.3	110.5	112.9	112.5	113.4	112.9	151.1	165.3	222.9	188.1	105.6	182.3	139.6	113.7	26.1	0.7
Nb	12.6	6.2	10.2	7.2	6.4	5.5	7.5	7.1	9.6	9.6	9.5	8.5	10.1	12.3	10.1	7.2	9.7	8.6	8.0	2.1	0.3
Mo	<0.2	0.4	0.6	0.4	0.4	0.9	<0.2	0.4	0.3	0.2	<0.2	0.3	0.4	0.7	0.8	0.3	0.6	0.4	0.5	0.3	0.2
Th	3.1	1.9	4.9	3.3	3.0	2.5	1.4	1.4	1.8	1.6	1.8	4.5	2.2	6.7	5.6	1.4	5.2	1.8	0.7	<0.3	0.3
U	0.5	0.7	1.1	0.7	0.5	0.6	0.7	<0.4	0.5	0.6	0.6	1.5	1.0	0.9	0.9	0.5	0.4	<0.4	<0.4	<0.4	0.4
Y	26.8	14.9	42.5	53.7	39.7	38.9	24.5	24.1	23.7	23.8	23.9	24.3	32.9	46.8	41.3	26.7	37.1	33.0	26.4	16.3	0.3
La	15.6	7.6	31.8	21.4	14.3	20.2	11.3	12.2	13.5	13.3	14.3	15.1	14.5	32.5	26.9	12.3	26.6	13.6	12.3	<1.7	1.7
Ce	34.4	18.5	70.1	50.5	31.9	38.8	24.8	25.4	27.6	29.5	30.1	38.5	34.5	74.4	56.9	27.6	57.4	32.1	28.4	4.1	2.1
Nd	22.8	9.9	38.0	34.8	24.8	24.6	16.3	16.5	18.7	18.2	19.8	19.6	21.2	39.3	31.3	16.9	29.2	20.5	19.6	2.1	2
Sm	5.4	3.1	8.5	9.6	6.2	7.3	5.0	4.4	5.1	3.1	4.3	4.3	6.3	6.8	7.6	2.2	5.6	5.9	3.9	<2	2

(continued)

Table 2. (Continued)

	SH1A	SH1B	SH2	SH3A	SH3B	SH4	SH5A	SH5B	SH5C	SH5D	SH5E	KR1	KR2	CSD1	CSD2	CSD3	CSD4	CSD5	CSD6	HC1	2σ
Yb	2.9	4.6	4.0	4.2	2.6	3.1	3.3	3.3	3.4	3.0	2.7	3.6	3.8	4.0	3.7	3.4	3.3	2.9	2.9	3.2	1.4
Hf	3.5	1.8	4.0	5.0	5.3	2.9	2.2	2.2	2.6	2.3	2.6	3.6	3.9	5.6	5.3	3.0	5.4	3.1	2.2	<1.4	1.4
Cs	2	<1.2	<1.2	<1.2	<1.2	<1.2	2	<1.2	2	3	2	<1.2	<1.2	2	2	2	<1.2	<1.2	2	4	1.2

Concentrations are reported on a volatile-free basis. Major elements have been normalized to Total = 100 wt% and trace element matrix corrections were performed using those values. All Fe is reported as Fe_2O_3. Data marked '<' indicate a measured value below the lower limit of detection. Estimated 2σ uncertainties are derived from multiple runs of a basaltic sample. LOI, Loss on Ignition; Trace sum is measured sum of trace elements expressed as oxides on a volatile-free basis, prior to normalization to 100 wt%; Total (*M*) is measured sum of major elements, expressed on a volatile-free basis prior to normalization, plus Trace sum; Total (*N*) is sum of major elements after normalization to 100 wt%.

Table 3. *Whole-rock geochemistry determined by inductively coupled plasma atomic emission and mass spectrometry*

	Inductively coupled plasma atomic emission spectrometry																						
	wt%												ppm										
	SiO_2	TiO_2	Al_2O_3	Fe_2O_3	MnO	MgO	CaO	Na_2O	K_2O	P_2O_5	Total (*N*)	Total (*M*)	Ba	Sr	Y	Zr	Co	Cr	Cu	Ni	Sc	V	Zn
SH5E	50.2	1.34	16.4	9.5	0.22	8.0	8.7	3.0	2.30	0.33	100.00	97.49	471.0	544.9	24.9	121.9	34.4	350.2	12.7	119.2	32.5	233.6	71.5
CSD5	49.5	3.13	14.4	12.9	0.24	6.7	8.1	3.6	1.02	0.34	100.00	98.59	287.5	498.3	31.8	155.9	58.1	143.5	76.7	58.4	48.8	363.0	143.1
2σ	0.42	0.03	0.22	0.16	0.01	0.13	0.19	0.14	0.03	0.02	–	–	3.4	2.6	0.4	3.3	2.3	4.0	4.6	0.8	1.2	2.8	2.9
	Inductively coupled plasma mass spectrometry (ppm)																						
	Nb	Mo	Cs	Hf	Ta	Pb	Th	U	La	Ce	Pr	Nd	Sm	Eu	Gd	Tb	Dy	Ho	Er	Tm	Yb	Lu	
SH5E	8.7	0.6	1.6	2.6	0.60	15.9	1.7	0.8	15.3	34.0	4.7	21.5	4.8	1.67	4.6	0.75	4.4	0.91	2.5	0.36	2.1	0.32	
CSD5	8.0	0.8	0.7	3.6	0.61	11.7	1.2	0.6	12.4	31.6	4.5	21.6	5.26	1.91	5.5	0.93	5.5	1.19	3.1	0.44	2.7	0.41	
2σ	0.4	0.08	0.02	0.2	0.05	0.2	0.1	0.04	0.2	0.1	0.1	0.3	0.1	0.02	0.1	0.03	0.1	0.03	0.03	0.02	0.1	0.01	

Concentrations are reported on a volatile-free basis. Major and trace elements have been normalized to Total = 100 wt%, by multiplying each value by [100/reported total] for ICP-AES and by [100/(100 – LOI)] for ICP-MS. (For LOI see Table 2.) Total (*M*) is measured sum of major elements, expressed on a volatile-free basis prior to normalization; total (*N*) is sum of major elements after normalization to 100 wt%. All Fe is reported as Fe_2O_3. Estimated 2σ uncertainties are derived from multiple runs of a basaltic sample.

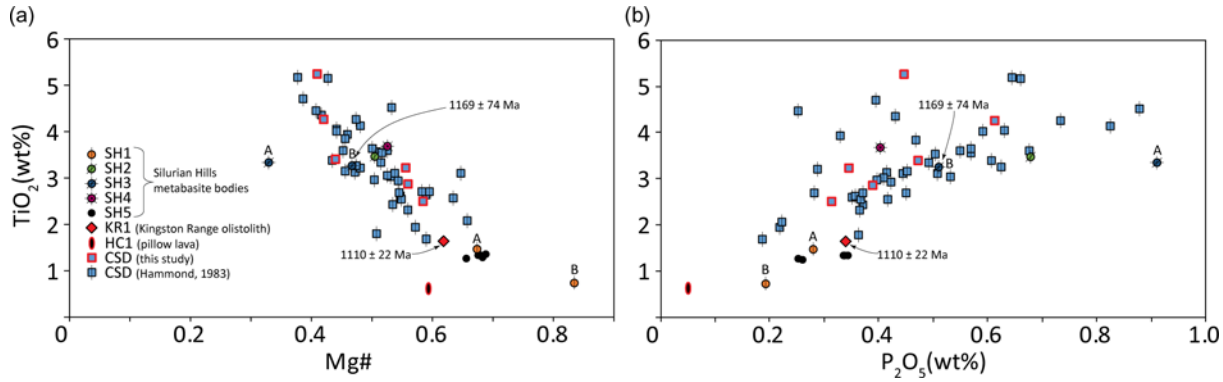

Fig. 7. Major elements of samples of this study and the Crystal Spring Diabase. (**a**) TiO_2 v. Mg# (mole ratio $Mg^{2+}/(Mg^{2+} + Fe^{2+})$). (**b**) TiO_2 v. P_2O_5. Crystal Spring Diabase (CSD) data from this study ($n = 6$) and Hammond (1983, $n = 42$). Adapted from figures 6 and 7 of Hammond (1986). Letters indicate along-strike samples.

composition (Piccoli & Candela 2002). All U–Pb apatite and zircon isotopic data, including standards and selected cathodoluminescence images, are reported in the supplementary material.

Apatites analysed from the Kingston Range olistolith, KR1, yielded a well-constrained isochron on Tera–Wasserburg concordia, with a lower intercept age of 1110 ± 22 Ma (MSWD = 3.2; $n = 83$, Fig. 11a) and an unanchored (i.e. solely constrained by the analytical data) $^{207}Pb/^{206}Pb$ initial ratio of 0.9514. This age is interpreted as recording the igneous crystallization of KR1. The Silurian Hills metabasite body, SH3B, displays more complicated U–Pb Tera–Wasserburg concordia systematics (Fig. 11b). The majority of the grains, depicted by the black ellipses, define a young lower intercept age of 78 ± 43 Ma (MSWD = 0.65; $n = 60$) with an unanchored $^{207}Pb/^{206}Pb$ initial ratio of 0.8475. Three grains, depicted by green ellipses, define a lower intercept age of 1169 ± 74 Ma (MSWD = 3.1) and an unanchored $^{207}Pb/^{206}Pb$ initial ratio of 0.9531. SH3B is interpreted as a *c.* 1.1 Ga metabasite, similar to sample KR1, but that has experienced variable and pervasive later

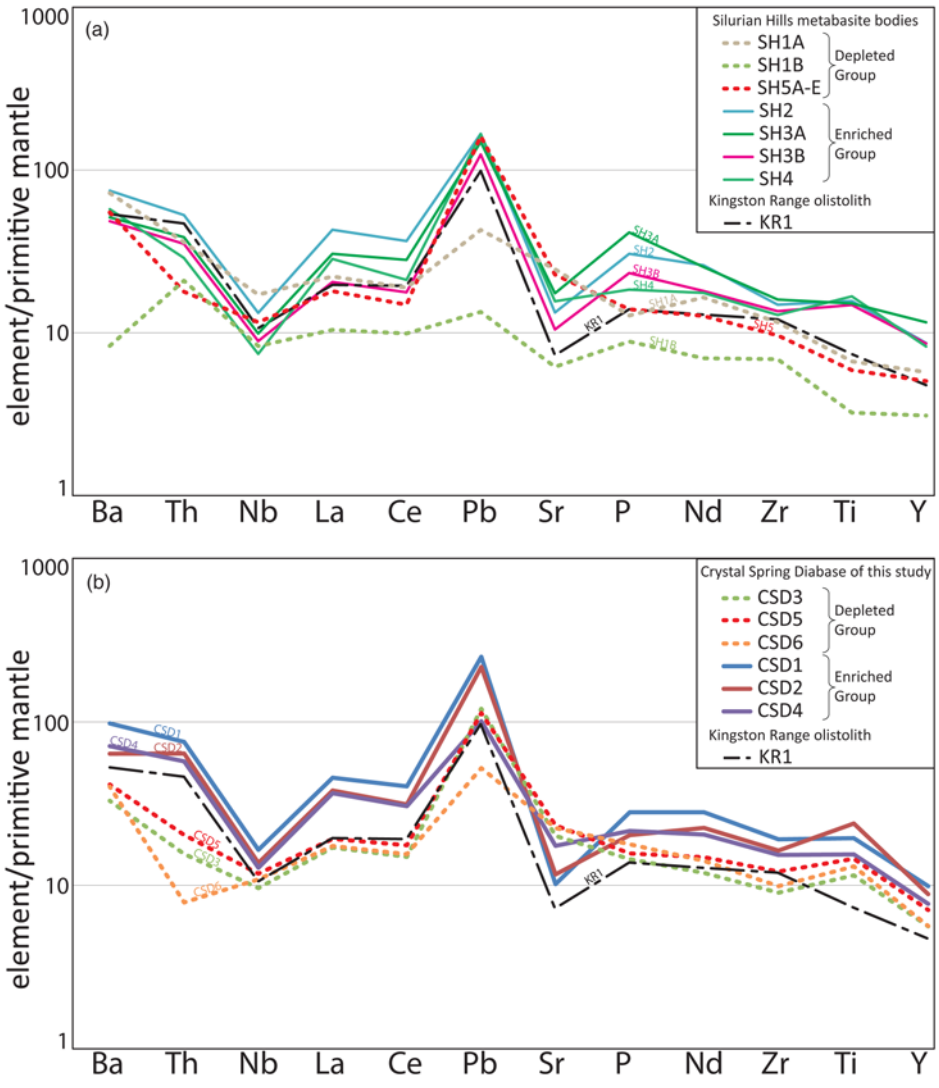

Fig. 8. XRF multi-element diagrams of primitive mantle normalized trace elements (Sun & McDonough 1989). (**a**) KPu metabasites from the Silurian Hills. SH5A–E is a mean of all SH5 XRF data. (**b**) CSD of this study. Kingston Range olistolith is included in both (**a**) and (**b**), to highlight common features. 'Enriched' and 'Depleted' trace element groups are indicated.

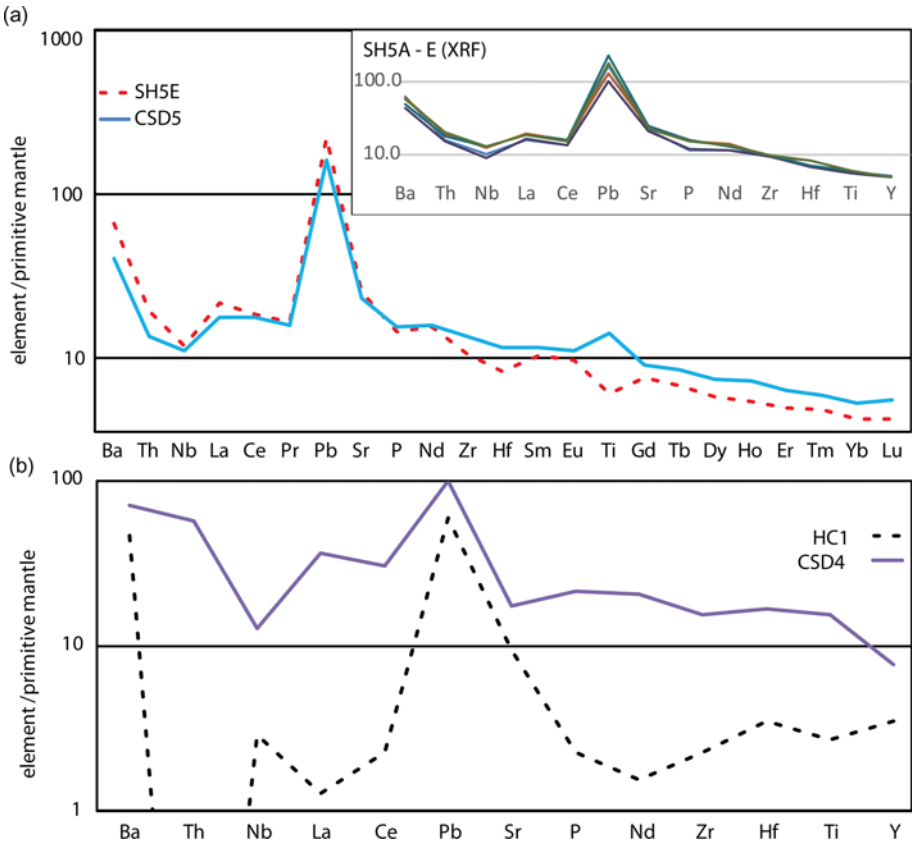

Fig. 9. Multi-element diagrams of primitive mantle normalized trace elements (Sun & McDonough 1989). (**a**) KPu metabasite body SH5E compared with the *in situ* Crystal Spring Diabase, CSD5. Both samples from the Silurian Hills, using ICP-MS and ICP-AES data. Inset shows XRF data demonstrating that all SH5 samples are near-identical. (**b**) Panamint Range pillow lava (HC1) compared with the *in situ* Crystal Spring Diabase from the Kingston range (CSD4).

Pb loss. This is evidenced by the range in ^{207}Pb-corrected ages in Figure 11c, which range from *c.* 1.1 Ga to the Cenozoic.

Apatites from the uppermost, dropstone-associated, metabasite body in the Silurian Hills, SH5, were characterized by problematically low U contents, resulting in large uncertainties. Despite this, a poorly constrained Tera–Wasserburg intercept could be discerned, tentatively suggesting a metamorphic or magmatic reset in late Cretaceous–Cenozoic time, similar to sample SH3B from the same metabasite body.

Twenty two zircons were recovered from the SH5 metabasite body. Thirteen are older than the CSD (1144–2595 Ma) and nine are younger (12–492 Ma). The age distribution of the older group is similar to that of detrital zircons of this study (Fig. 12) and inherited zircons of Shastri *et al.* (1991), from within Arizonan mafic SWLLIP dykes. Only one zircon had significant age zonation, with concordia ages of 492 ± 25 Ma (rim) and 1121 ± 24 Ma (core). Interpretation of the zircon dataset is however problematic. Sample SH5 was separated and analysed in two laboratories. Each yielded a 12.6 Ma zircon, which is significantly younger than the most recent amphibolite-facies (i.e. the assemblage of SH5) metamorphic event in the region (*c.* 90 Ma; DeWitt *et al.* 1984). Zircon is usually highly undersaturated in basaltic melts (Dickinson & Hess 1982). This explains the extremely low zircon yield in sample SH5, but also makes it highly vulnerable to contamination. We suggest therefore that recent loose sediment, trapped within a fracture or a very thin duricrust, may be the origin of these anomalously young ages. In summary, although the majority of the zircon ages are probably inherited, contamination cannot be unequivocally ruled out, and hence the zircon data provide no conclusive geochronological constraint.

Detrital zircon geochronology of the Crystal Spring and Horse Thief Springs Formations

Detrital zircons were sampled from the basal conglomerate of the Crystal Spring Formation, in the Black Mountains (DZ-BM1) and Silurian Hills (DZ-SH1), and from its overlying Arkose Member (DZ-SH2) in the Silurian Hills only (Table 1). Additionally, DZ-SH3 is from unit P6 of the Silurian Hills and has been tentatively assigned a position either below (Maud 1979, p. 17) or above (Smith *et al.* 2016) the Crystal Spring unconformity. All samples, except DZ-SH3, yielded unimodal age spectra, consistent with those reported from the Crystal Spring Formation in the Kingston Range (MacLean 2007; Mahon *et al.* 2014*a*) (Fig. 12). Smaller secondary peaks in these data, from 1320 Ma (DZ-SH2) to 1400 Ma (DZ-SH1), are present but less pronounced in the published Crystal Spring data. DZ-SH3, conversely, yielded an age spectrum very similar to those from above the Crystal Spring unconformity throughout the region, including the Silurian Hills samples of Smith *et al.* (2016) (Fig. 12). These data suggest that a distinct Crystal Spring Formation detrital zircon age signature may be recognized in separate localities around the region and used as a correlation tool. In the Silurian Hills, this approach places the unconformity below unit P6. Furthermore, these data determine a new maximum depositional age for the Pahrump Group, of 1371 ± 14 Ma, using the YC2σ(3+) statistical approach of Dickinson & Gehrels (2009). This is based upon the five youngest zircon grains overlapping in age at 2σ uncertainty, from DZ-SH1, 1 m above the base of the Pahrump Group in the Silurian Hills. It should be noted that the three youngest grains from sample K03DV04 (*c.* 1320 Ma; Mahon *et al.* 2014*a*) (Fig. 12) are from a different and younger depositional system (Roberts 1974, 1976; Mahon *et al.* 2014*a*) and therefore do not reflect a maximum age for the Pahrump Group (see Mulder *et al.* 2017).

Discussion

Isotopic age and geochemical data suggest that the Silurian Hills KPu metabasites have ages of around 1.1 Ga and are genetically related to the CSD. This challenges conventional wisdom by suggesting two possibilities: (1) the Silurian Hills glacial deposits

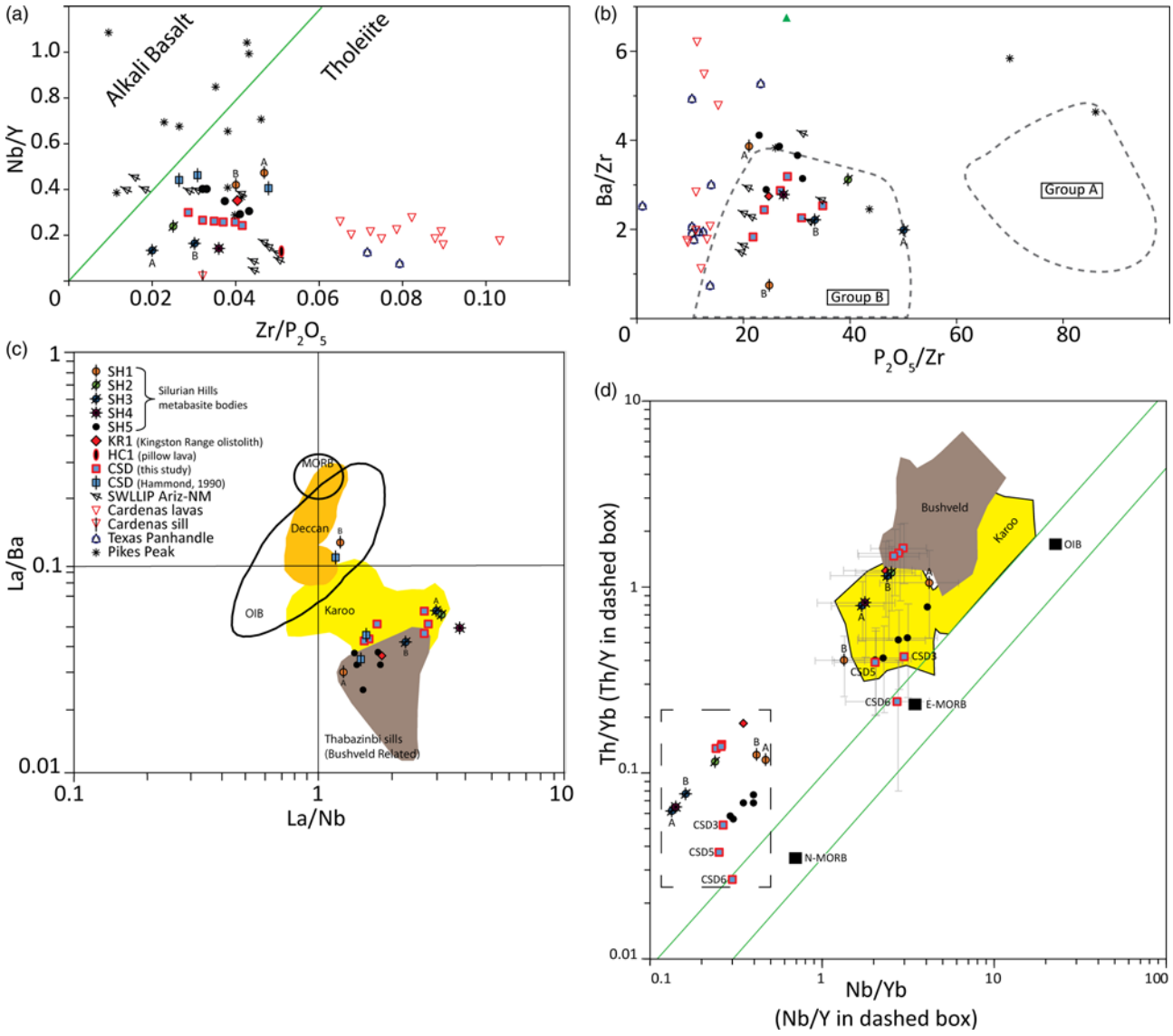

Fig. 10. Elemental ratios of this study compared with samples of the SWLLIP (figs. a - b) and other large igneous provinces (figs. c - d). (**a**) Nb/Y v. Zr (ppm)/P_2O_5 (ppm), alkali basalt/tholeiite discrimination plot adapted from Winchester & Floyd (1976, fig. 11). (**b**) Ba/Zr v. P_2O_5 (ppm)/Zr (ppm), adapted from an SWLLIP parental magma discrimination plot of Hammond (1990, Fig. 8). (**c**) La/Ba v. La/Nb, adapted from Ernst (2014, fig. 10.14). (**d**) Th/Yb v. Nb/Yb (and Th/Y v. Nb/Y in dashed box only), adapted from Pearce (2008, fig. 2) and Ernst (2014, fig. 10.7). Parallel straight lines define relatively uncontaminated magmas (e.g. OIB). E-MORB, enriched mid-ocean ridge basalt. Error bars: 2σ (Table 2). Uncertainty is significantly less for Th/Y v. Nb/Y and bars are omitted. SH5E and CSD5 are ICP-AES or ICP-MS data; remaining samples are XRF. SWLLIP Ariz–NM: mafic intrusive SWLLIP samples, forming a discontinuous belt from the Colorado River Trough (California–Arizona border) to Burro Mountains (SW New Mexico) (Hammond 1990; Bright *et al.* 2014), excluding one outlier, the Antelope Hills in (**a**). Cardenas Lavas and Cardenas Sill: mafic lavas and a sill from the Grand Canyon (Larson *et al.* 1994). Texas Panhandle: mafic core from well Bivins99R (Li *et al.* 2007). Pikes Peak: mafic intrusions from within a felsic batholith, central Colorado (Smith *et al.* 1999).

are part of the Mesoproterozoic Crystal Spring Formation and therefore *c.* 400 myr older than previously thought; or (2) the metabasite bodies represent olistoliths that were transported *c.* 400 myr after crystallization.

The former hypothesis, first suggested by Kupfer (1960), would be plausible given the correlation uncertainties in the Silurian Hills. However, detrital zircon data of this study place the Crystal Spring unconformity hundreds of metres below the KPu in the Silurian Hills. This confirms the existing consensus (e.g. Basse 1978; Maud 1979; Shafer 1983; Smith *et al.* 2016) and renders a Mesoproterozoic glaciation unlikely.

The latter hypothesis is well precedented in the southern Kingston Range, where field observation alone allowed an olistolith interpretation (Calzia *et al.* 2000). This is supported herein by the U–Pb age and geochemistry of sample KR1. By contrast, in the Silurian Hills, reliance on field observation alone has hitherto allowed the sill interpretation to remain unchallenged. This is despite carbonate olistoliths, in the KPu of the Silurian Hills, alerting us to the possibility of metabasite olistoliths (Fig. 2a). Likewise, along-strike disaggregation and brecciation of metabasite bodies into fragments within the surrounding sediments could suggest erosion potentially resulting from transport. Importantly, however, this same field observation is equally consistent with a sill interpretation. Indeed, Kupfer suggested that the depth at which sills were intruded decreased upwards in the section, possibly to the point of extrusion. He also noted that sedimentary fragments of the same material occurred above the shallowest of these sills (Kupfer 1960, p. 199). In this context, the exhumation and reworking of a shallow sill into sedimentary fragments within the overlying strata would appear a parsimonious explanation. Only using U–Pb age and geochemical comparison with the CSD is it possible to conclude that the Silurian Hills metabasite bodies are in fact olistoliths.

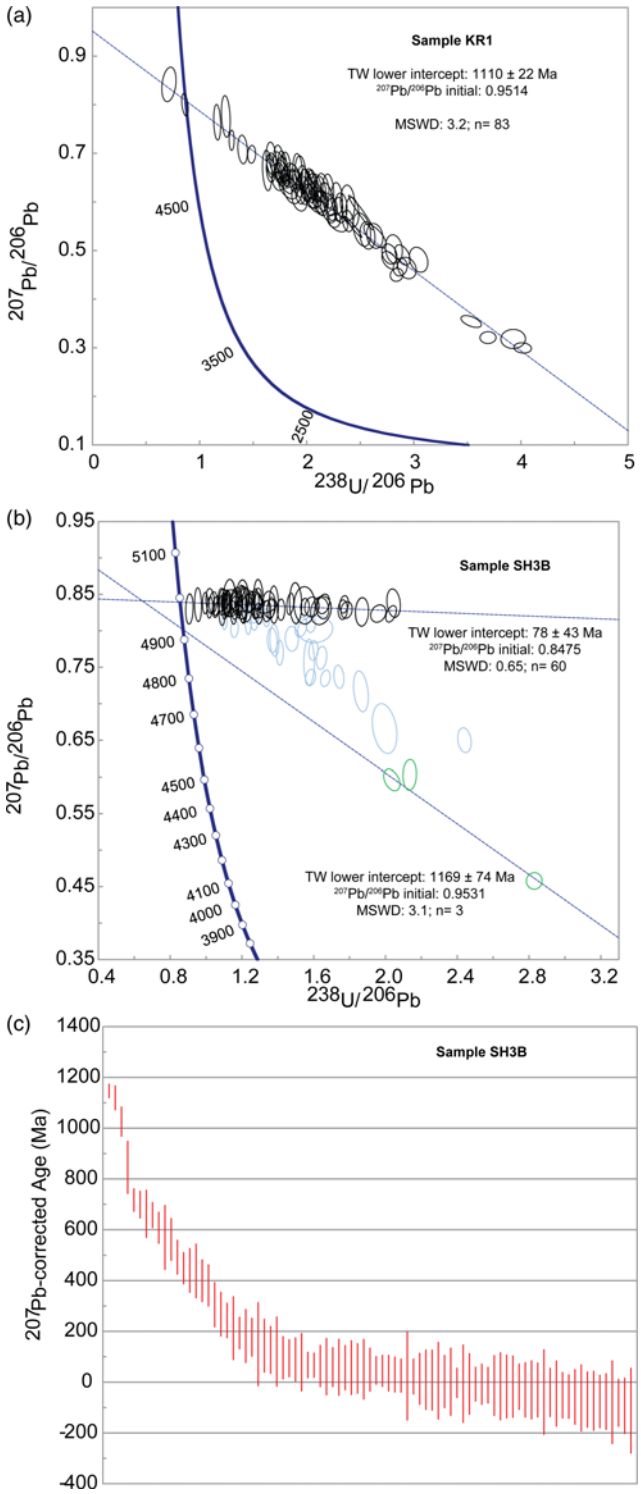

Fig. 11. Geochronology of KPu metabasite apatites. (**a**) U–Pb Tera–Wasserburg lower intercept age for the Kingston Range olistolith, KR1. (**b**) U–Pb Tera–Wasserburg lower intercept ages for Silurian Hills metabasite body, SH3B. The younger intercept age is calculated from the black ellipses whereas the older intercept age is calculated from the green ellipses. The $^{207}Pb/^{206}Pb$ initial ratios in (**a**) and (**b**) are calculated from the data obtained in this study. (**c**) ^{207}Pb-corrected ages for sample SH3B. The initial Pb composition is calculated using the Stacey & Kramers (1975) terrestrial Pb evolution model, using an iterative approach described by Chew *et al.* (2011).

The uppermost metabasite body in the Silurian Hills, SH5, is however problematic. It is an *in situ* sill that cross-cuts, and therefore postdates, dropstone-bearing strata (Fig. 4). This strongly suggests that it is of Cryogenian or younger age. However, its composition is very similar indeed to the *in situ* CSD of the Silurian Hills (Fig. 10a), which predates the Cryogenian by over 300 myr. Either two near-identical magmas were produced in the Silurian Hills, over 300 myr apart, or SH5 is enclosed within an olistolith of ≥1.1 Ga dropstone-bearing strata, which correlate with the Crystal Spring unconformity. The former is more likely for three reasons. First, the Crystal Spring Formation, and correlatives on the SW Laurentian margin, has not yielded any dropstones or glacial evidence (e.g. Roberts 1974, 1976; Mulder *et al.* 2017). Second, the country rock of SH5 is a similar facies to other KPu strata, at least in the Silurian Hills (Le Heron *et al.* 2017). Third, the presence of ≪1.1 Ga zircons within SH5 is consistent with a young sill.

SH1 and SH5 are the only Silurian Hills metabasite bodies that are members of (1) the depleted trace element group (Fig. 8a), (2) the low-Ti group (Table 2, Fig. 7) and (3) the higher grade mineral assemblage group. Given these similarities, and the interpretation of SH5 as a ≪1.1 Ga sill, we must therefore consider whether SH1 may also be a 'young' sill. However, countering each one of these similarities in turn: (1) Several CSD samples also belong to the depleted trace element group (Fig. 8b); (2) the Kingston Range olistolith has similarly depleted Ti (Table 2, Fig. 7); (3) the higher grade mineral assemblage occurs in published CSD (Hammond 1983) and the CSD of this study (CSD5, -6). Furthermore, the outcrop character of SH1 is more akin to the other metabasite bodies than it is to SH5. It is more poorly preserved, with no intact lower margin and it lacks cross-cutting relationships. Therefore a *c.* 1.1 Ga age for SH1 seems marginally more likely. This uncertainty illustrates the potential interpretative difficulties of such metabasite bodies, even when geochemical data are available.

One potential source of the Silurian Hills metabasite bodies is the CSD at Saratoga Springs (Fig. 1). There it is truncated by the Crystal Spring unconformity and reworked into the basal conglomerate of the Horse Thief Springs Formation (Mahon *et al.* 2014*b*). It is, however, possible that olistoliths were transported in from multiple localities, as outlined above in relation to the lower and higher metamorphic grade groups of the Silurian Hills metabasite bodies. However, can such a suggestion be reconciled with the local source and minimal transport of olistoliths that Le Heron *et al.* (2017) suggested? Perhaps there was minimal olistolith transport, but considerable tectonic juxtaposition, between emplacement of the stratigraphically lowest and highest metabasite bodies. If so, then the metasedimentary packages separating olistostromes in the Silurian Hills (Fig. 2a) may each indicate a significant period of elapsed time. Alternatively, the metabasite bodies may have been transported kilometres by glacial action, perhaps ultimately as ice-rafted debris. Both these suggestions are speculative, but serve to reinforce the potential complexity of interplay between glacial-related and rift-related sedimentation (see Le Heron *et al.* 2017).

The KPu is an important element in reconstructing the rifting of the SW Laurentian margin (Macdonald *et al.* 2013; Yonkee *et al.* 2014). At its western extremity, the tholeiitic pillow lavas of the Panamint Range are commonly cited as evidence of a rift signature during the Cryogenian (e.g. Miller 1985; Prave 1999; Smith *et al.* 2016). At its southeastern extremity, the 'sills' of the Silurian Hills have similarly been cited as evidence for active tectonics during KPu deposition (Basse 1978, p. 53). No other Cryogenian magmatism has been confirmed from the remaining Pahrump Group. Therefore, reinterpreting the Silurian Hills sills as olistoliths significantly reduces the areal extent of Cryogenian magmatism for this section of the SW Laurentian margin. In this context, establishing whether there are indeed any Cryogenian-age magmas in the Death Valley area, outside the Panamint Range, becomes a priority.

The features found in the metabasite bodies of the Silurian Hills may be found in other Precambrian extensional settings; for example, metabasite bodies reported by Tembo *et al.* (1999) from

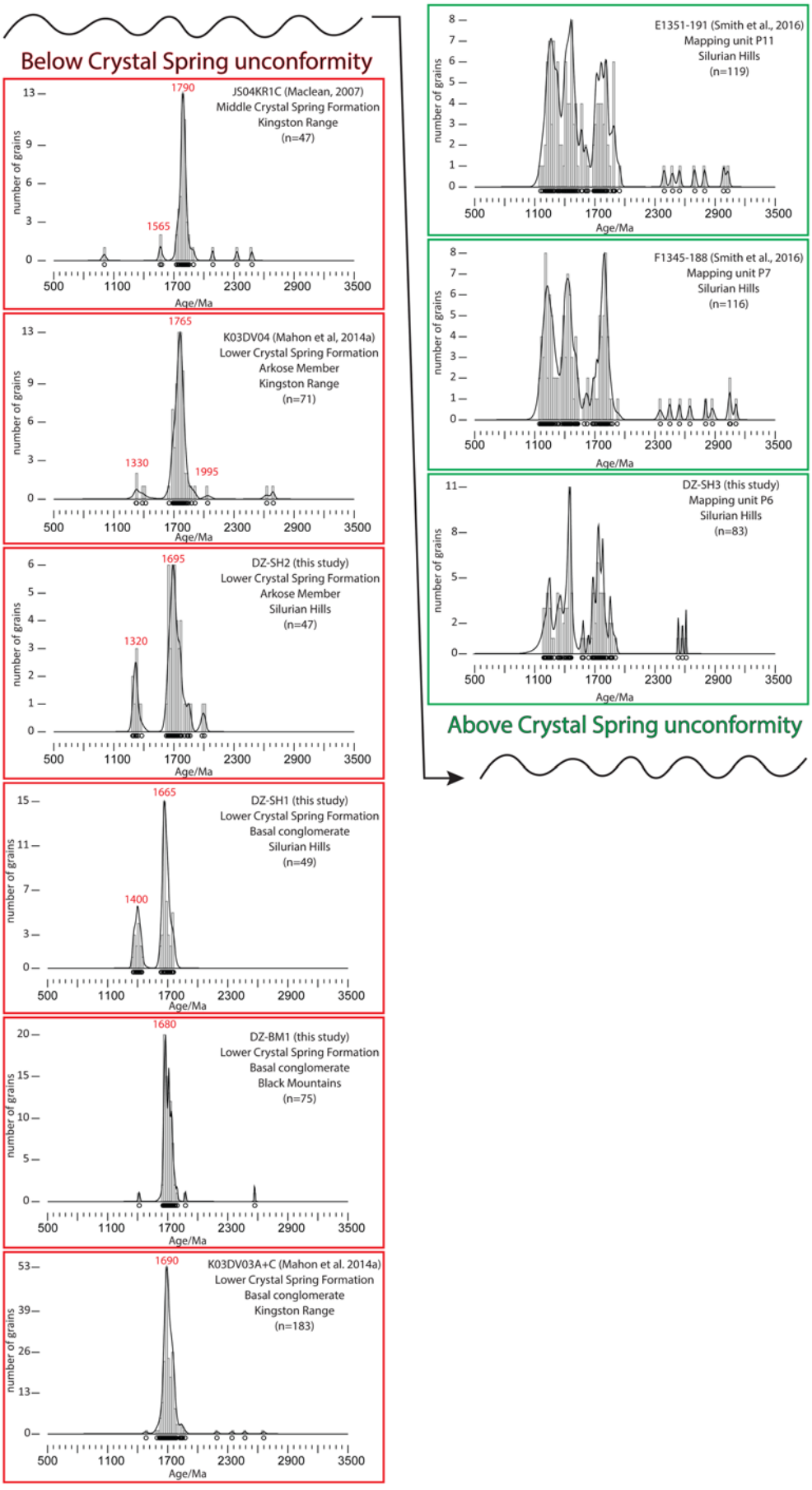

Fig. 12. Relative probability plots and histograms of detrital zircon samples. Left: All published data and samples of this study from the Crystal Spring formation, from across the region. Right: All published data and samples of this study from between the Crystal Spring unconformity and the base of the KPu, from the Silurian Hills only. The distinctly different spectra above and below the unconformity should be noted. Histograms use 20 Ma bin size, with number of grains indicated on *y*-axis. Probability plots were created using Density Plotter 7.3 (Vermeesch 2012). Data of discordance >10% discarded. For MacLean (2007) both LA-ICP-MS and SHRIMP (sensitive high-resolution ion microprobe) data were used. Crystal Spring Formation data of Mulder *et al.* (2017) were not used.

Neoprototerozoic strata of the Lufilian belt, Zambia. These basaltic rocks crop out as small bouldery hillocks and were assumed to be *in situ* with their country rock. They are hosted within breccia and become locally brecciated themselves. They are not reported cross-cutting country rock. These features are reminiscent of the boulder-like outcrops (Fig. 3e) and along-strike disaggregation (Fig. 3b) in the Silurian Hills, along with the continuum from intact olistolith, through mafic breccia, to conglomerate in the Kingston Range (Fig. 5b–f). These characteristics encompass almost all of the field observations that support reinterpretation of the metabasite bodies in the Silurian Hills. Despite this, we do not suggest that an immediate reinterpretation as olistoliths is required in the Lufilian belt. Indeed, these same key field observations are reported from the pillow lavas of the Panamint Range, which have not been remobilized. Instead, this serves to reiterate that it may be impossible to discern sill from olistolith, based on field observation alone, and that this problem may occur elsewhere. Furthermore, this difficulty may be exacerbated in Precambrian rocks, where there is a lack of geochronological fossil markers. Indeed, we ourselves believed the Silurian Hills metabasite bodies to be sills, intruded into shallow wet sediments then shortly afterwards exhumed and reworked. It was in this context that we originally sampled these metabasites, to obtain an age for the Cryogenian in Death Valley. We realized our mistake only when we obtained Mesoproterozoic ages by LA-ICP-MS. This paper therefore acts as a cautionary exemplar of how readily large-scale igneous bodies, within extensional tectonic settings, may be misinterpreted.

Conclusions

(1) New field data compare metabasites from three KPu localities: an olistolith in the Kingston Range, an *in situ* pillow lava in the Panamint Range and metabasite bodies in the Silurian Hills. We find morphological similarities between the three, including brecciation, along-strike disaggregation and boulder-like outcrops. In the Silurian Hills these observations support a sill interpretation, but do not preclude an olistolith interpretation. The exception is the uppermost metabasite body of the Silurian Hills, which cross-cuts country rock strata and is undoubtedly an in situ intrusion.

(2) Whole-rock geochemistry suggests that all KPu and CSD metabasite samples are comagmatic. The exception is the Panamint Range pillow lava, which has no clear geochemical relationship to other samples of this study.

(3) Apatite U–Pb ages from the metabasite bodies of the Silurian Hills (1169 ± 74 Ma) and the Kingston Range olistolith (1110 ± 22 Ma), reported herein, are similar to the published age of the CSD and within error of the SWLLIP. Conversely, these ages are over 300 myr older than the depositional age of the enclosing metasedimentary strata of the KPu.

(4) We conclude that metabasite bodies in the KPu of the Silurian Hills, except the uppermost, despite having been previously interpreted as sills, are in fact olistoliths. Importantly, their outcrop characteristics are consistent with a sill interpretation, and it is only through geochemical and isotopic analysis that their true identity is revealed.

(5) As olistolith and magma production are both commonly associated with extensional tectonic settings, we suggest that such misidentification could occur elsewhere and illustrate this with an example from the literature.

(6) This paper serves to warn others against the interpretative difficulties of olistoliths masquerading as sills.

Acknowledgements The authors would like to thank C. Zalunardo, A. L. Woodworth, J. E. Comstock, A. R. Prave, R. E. Ernst, I. J. Fairchild, M. Lechte, and C. and M. Kienitz for their kind help. We thank two anonymous reviewers, R. C. Mahon and J. Wakabayashi for extensive insights that have greatly improved this work.

Funding T.M.V. benefited from the Robert Scott Memorial Award (CASP) and Crowther Fund (Open University). The Arizona Laserchron Center is supported by NSF EAR-1338583. Analyses from Trinity College Dublin were supported by Science Foundation Ireland under Grant Numbers 12/IP/1663 and 15/IACA/3365, awarded to D.M.C. S.R.C. was funded by a Small Research Grant from the Office of Research and Special Programs at the University of Wisconsin-Eau Claire.

Scientific editing by Tyrone Rooney

References

Albee, A.L., Labotka, T.C., Lanphere, M.A. & McDowell, S.D. 1981. *Geologic Map of the Telescope Peak Quadrangle, 1:62,500, GQ-1532*. US Geological Survey, Reston, VA.

Basse, R.A. 1978. *Stratigraphy, Sedimentology, and Depositional Setting of the Late Precambrian Pahrump Group, Silurian Hills, California*. MS thesis, Stanford University, Stanford, CA.

Bright, R.M., Amato, J.M., Denyszyn, S.W. & Ernst, R.E. 2014. U–Pb geochronology of 1.1 Ga diabase in the southwestern United States: Testing models for the origin of a post-Grenville large igneous province. *Lithosphere*, **6**, 135–156, https://doi.org/10.1130/L335.1

Busfield, M.E. & Le Heron, D.P. 2015. A Neoproterozoic ice advance sequence, Sperry Wash, California. *Sedimentology*, https://doi.org/10.1111/sed.12210

Calzia, J.P., Troxel, B.W., Wright, L.A., Burchfiel, B.C., Davis, G.A. & McMackin, M.R. 2000. *Geologic Map of the Kingston Range, Southern Death Valley, California. 1:31,680*. US Geological Survey, Open-File Report, **00-412**.

Carlisle, D. 1963. Pillow breccias and their aquagene tuffs, Quadra Island, British Columbia. *Journal of Geology*, **71**, 48–71, https://doi.org/10.1086/626875

Chew, D.M., Sylvester, P.J. & Tubrett, M.N. 2011. U–Pb and Th–Pb dating of apatite by LA-ICPMS. *Chemical Geology*, **280**, 200–216, https://doi.org/10.1016/j.chemgeo.2010.11.010

Chumakov, N.M. 2011. Glacial deposits of the Baykonur Formation, Kazakhstan and Kyrgyzstan. *In*: Arnaud, E., Halverson, G.P. & Shields-Zhou, G. (eds) *The Geological Record of Neoproterozoic Glaciations*. *Geological Society, London, Memoirs*, **36**, 303–307, https://doi.org/10.1144/M36.26

Creveling, J.R., Bergmann, K.D. & Grotzinger, J.P. 2016. Cap carbonate platform facies model, Noonday Formation, SE California. *Geological Society of America Bulletin*, **128**, 1249–1269, https://doi.org/10.1130/B31442.1

DePaolo, D. 1981. Trace-element and isotopic effects of combined wallrock assimilation and fractional crystallization. *Earth and Planetary Science Letters*, **53**, 189–202, https://doi.org/10.1016/0012-821X(81)90153-9

DeWitt, E.D., Armstrong, R.L., Sutter, J.F. & Zartman, R.E. 1984. U–Th–Pb, Rb–Sr, and Ar–Ar mineral and whole-rock isotopic systematics in a metamorphosed granitic terrane, southeastern California. *Geological Society of America Bulletin*, **95**, 723–739, https://doi.org/10.1130/0016-7606(1984)95%3C723:URAAMA%3E2.0.CO;2

Dickinson, W.R. & Gehrels, G.E. 2009. Use of U–Pb ages of detrital zircons to infer maximum depositional ages of strata: a test against a Colorado Plateau Mesozoic database. *Earth and Planetary Science Letters*, **288**, 115–125, https://doi.org/10.1016/j.epsl.2009.09.013

Dickinson, J.E. & Hess, P.C. 1982. Zircon saturation in lunar basalts and granites. *Earth and Planetary Science Letters*, **57**, 336–344, https://doi.org/10.1016/0012-821X(82)90154-6

Ernst, R.E. 2014. *Large Igneous Provinces*. Cambridge University Press, Cambridge.

Eyles, N. & Januszczak, N. 2004. 'Zipper-rift': a tectonic model for Neoproterozoic glaciations during the breakup of Rodinia after 750 Ma. *Earth-Science Reviews*, **65**, 1–73, https://doi.org/10.1016/S0012-8252(03)00080-1

Festa, A., Dilek, Y., Pini, G.A., Codegone, G. & Ogata, K. 2012. Mechanisms and processes of stratal disruption and mixing in the development of mélanges and broken formations: Redefining and classifying mélanges. *Tectonophysics*, **568**, 7–24, https://doi.org/10.1016/j.tecto.2012.05.021

Fouts, J.A. 1974. *Petrology and Chemistry of Some Diabase Sills in Central Arizona*. PhD thesis, University of Arizona, Tucson.

Hammond, J.L.G. 1983. *Late Precambrian Diabase Intrusions in the Southern Death Valley Region, California: Their Petrology, Geochemistry, and Tectonic Significance*. PhD thesis, University of Southern California, Los Angeles.

Hammond, J. 1986. Geochemistry and petrogenesis of Proterozoic diabase in the southern Death Valley region of California. *Contributions to Mineralogy and Petrology*, **93**, 312–321, https://doi.org/10.1007/BF00389390

Hammond, J.G. 1990. Middle Proterozoic diabase intrusions in the southwestern USA as indicators of limited extensional tectonism. *In*: Ryan, A.B., Rivers, T. & Gower, C.F. (eds) *Mid-Proterozoic Laurentia–Baltica*. Geological Association of Canada, Special Papers, **38**, 517–531.

Hazzard, J.C. 1939. Possibility of a pre-Cambric glaciation in southeastern California. *Pan-American Geologist*, **71**, 47–48.

Heaman, L. & Grotzinger, J. 1992. 1.08 Ga diabase sills in the Pahrump Group, California – implications for development of the Cordilleran miogeocline.

Geology, **20**, 637–640, https://doi.org/10.1130/0091-7613(1992)020<0637:GDSITP>2.3.CO;2

Hendricks, J.D. & Lucchitta, I. 1974. Upper Precambrian igneous rocks of the Grand Canyon, Arizona. *In*: Karlstrom, T.N.V., Swann, G.A. & Eastwood, R. L. (eds) *Geology of Northern Arizona with Notes on Archaeology and Paleoclimate*. Geological Society of America, Rocky Mountain Section, 65–86.

Jourdan, F., Bertrand, H., Féraud, G., Le Gall, B. & Watkeys, M.K. 2009. Lithospheric mantle evolution monitored by overlapping large igneous provinces: case study in southern Africa. *Lithos*, **107**, 257–268, https://doi.org/10.1016/j.lithos.2008.10.011

Kargi, H. & Barnes, C.G. 1995. A Grenville-age layered intrusion in the subsurface of west Texas: Petrology, petrography, and possible tectonic setting. *Canadian Journal of Earth Sciences*, **32**, 2159–2166, https://doi.org/10.1139/e95-168

Kupfer, D. 1960. Thrust faulting and chaos structure, Silurian Hills, San Bernardino County, California. *Geological Society of America Bulletin*, **71**, 181–214, https://doi.org/10.1130/0016-7606(1960)71[181:TFACSS]2.0.CO;2

Labotka, T., Albee, A., Lanphere, M. & McDowell, S. 1980. Stratigraphy, structure, and metamorphism in the central Panamint Mountains (Telescope Peak Quadrangle), Death Valley area, California – summary. *Geological Society of America Bulletin*, **91**, 125–129, https://doi.org/10.1130/0016-7606(1980)91<125:SSAMIT>2.0.CO;2

Larson, E., Patterson, P. & Mutschler, F. 1994. Lithology, chemistry, age, and origin of the Proterozoic Cardenas Basalt, Grand Canyon, Arizona. *Precambrian Research*, **65**, 255–276, https://doi.org/10.1016/0301-9268(94)90108-2

Le Heron, D.P., Busfield, M.E. & Prave, A.R. 2014. Neoproterozoic ice sheets and olistoliths: multiple glacial cycles in the Kingston Peak Formation, California. *Journal of the Geological Society, London*, **171**, 525–538, https://doi.org/10.1144/jgs2013-130

Le Heron, D.P., Tofaif, S., Vandyk, T. & Ali, D.O. 2017. A diamictite dichotomy: Glacial conveyor belts and olistostromes in the Neoproterozoic of Death Valley. *Geology*, https://doi.org/10.1130/G38460.1

Le Heron, D.P., Busfield, M.E., Ali, D.O., Al Tofaif, S. & Vandyk, T.M. 2018. The Cryogenian record in the southern Kingston Range, California: The thickest Death Valley succession in the hunt for a GSSP. *Precambrian Research*, in press, https://doi.org/10.1016/j.precamres.2017.07.017

Li, Y., Barnes, M.A., Barnes, C.G. & Frost, C.D. 2007. Grenville-age A-type and related magmatism in southern Laurentia, Texas and New Mexico, USA. *Lithos*, **97**, 58–87, https://doi.org/10.1016/j.lithos.2006.12.010

Li, Z.-X., Evans, D.A. & Halverson, G.P. 2013. Neoproterozoic glaciations in a revised global palaeogeography from the breakup of Rodinia to the assembly of Gondwanaland. *Sedimentary Geology*, **294**, 219–232, https://doi.org/10.1016/j.sedgeo.2013.05.016

Macdonald, F.A., Prave, A.R. *et al.* 2013. The Laurentian record of Neoproterozoic glaciation, tectonism, and eukaryotic evolution in Death Valley, California. *Geological Society of America Bulletin*, **125**, 1203–1223, https://doi.org/10.1130/B30789.1

MacLean, J.S. 2007. *Detrital-Zircon Geochronologic Provenance Analyses That Test and Expand the East Siberia–West Laurentia Rodinia Reconstruction*. PhD thesis, University of Montana, Missoula.

MacLean, J.S., Sears, J.W., Chamberlain, K.R., Khudoley, A.K., Prokopiev, A. V., Kropachev, A.P. & Serkina, G.G. 2009. Detrital zircon geochronologic tests of the SE Siberia–SW Laurentia paleocontinental connection. *Stephan Mueller Special Publication*, **4**, 111–116, https://doi.org/10.5194/smsps-4-111-2009

Mahon, R.C., Dehler, C.M., Link, P.K., Karlstrom, K.E. & Gehrels, G.E. 2014*a*. Detrital zircon provenance and paleogeography of the Pahrump Group and overlying strata, Death Valley, California. *Precambrian Research*, **251**, 102–117, https://doi.org/10.1016/j.precamres.2014.06.005

Mahon, R.C., Dehler, C.M., Link, P.K., Karlstrom, K.E. & Gehrels, G.E. 2014*b*. Geochronologic and stratigraphic constraints on the Mesoproterozoic and Neoproterozoic Pahrump Group, Death Valley, California: A record of the assembly, stability, and breakup of Rodinia. *Geological Society of America Bulletin*, **126**, 652–664, https://doi.org/10.1130/B30956.1

Maud, R.L. 1979. *Stratigraphy and Depositional Environments of the Carbonate–Terrigenous Member of the Crystal Spring Formation, Death Valley, California*. MS thesis, Pennsylvania State University, State College.

Maud, R.L. 1983. *Stratigraphy, Petrography and Depositional Environments of the Carbonate–Terrigenous Member of the Crystal Spring Formation, Death Valley, California*. PhD thesis, Pennsylvania State University, State College.

Miller, J.M.G. 1983. *Stratigraphy and Sedimentology of the Upper Proterozoic Kingston Peak Formation, Panamint Range, Eastern California*. PhD thesis, University of California, Santa Barbara.

Miller, J.M.G. 1985. Glacial and syntectonic sedimentation: The upper Proterozoic Kingston Peak Formation, southern Panamint Range, eastern California. *Geological Society of America Bulletin*, **96**, 1537–1553, https://doi.org/10.1130/0016-7606(1985)96<1537:GASSTU > 2.0.CO;2

Mrofka, D.D. 2010. *Competing Models for the Timing of Cryogenian Glaciation: Evidence from the Kingston Peak Formation, Southeastern California*. PhD thesis, University of California, Riverside.

Mulder, J.A., Karlstrom, K.E. *et al.* 2017. The syn-orogenic sedimentary record of the Grenville Orogeny in southwest Laurentia. *Precambrian Research*, **294**, 33–52, https://doi.org/10.1016/j.precamres.2017.03.006

Pearce, J.A. 2008. Geochemical fingerprinting of oceanic basalts with applications to ophiolite classification and the search for Archean oceanic crust. *Lithos*, **100**, 14–48, https://doi.org/10.1016/j.lithos.2007.06.016

Petterson, R., Prave, A.R., Wernicke, B.P. & Fallick, A.E. 2011. The Neoproterozoic Noonday Formation, Death Valley region, California. *Geological Society of America Bulletin*, **123**, 1317–1336, https://doi.org/10.1130/B30281.1

Piccoli, P.M. & Candela, P.A. 2002. Apatite in igneous systems. *In*: Kohn, M.L., Rakovan, J. & Hughes, J.M. (eds) *Phosphates – Geochemical, Geobiological, and Materials Importance*. Mineralogical Society of America and Geochemical Society, Reviews in Mineralogy and Geochemistry, **48**, 255–292, https://doi.org/10.2138/rmg.2002.48.6

Prave, A. 1999. Two diamictites, two cap carbonates, two $\delta^{13}C$ excursions, two rifts: The Neoproterozoic Kingston Peak Formation, Death Valley, California. *Geology*, **27**, 339–342, https://doi.org/10.1130/0091-7613(1999)027<0339:TDTCCT>2.3.CO;2

Roberts, M.T. 1974. *The Stratigraphy and Depositional Environments of the Lower Part of the Crystal Spring Formation*. PhD thesis, Pennsylvania State University, State College.

Roberts, M.T. 1976. Stratigraphy and depositional environments of the Crystal Spring Formation, Southern Death Valley region, California. *In*: Troxel, B.W. (ed.) *Geologic Features—Death Valley, California*. California Division of Mines and Geology, Special Report, **106**, 35–44.

Robertson, A.H.F. 1977. The Moni Mélange, Cyprus: an olistostrome formed at a destructive plate margin. *Journal of the Geological Society, London*, **133**, 447–466, https://doi.org/10.1144/gsjgs.133.5.0447

Shafer, D.C. 1983. *Petrology and Depositional Environments of the Beck Spring Dolomite, Southern Death Valley Region, California*. MS thesis, University of California, Davis.

Shapiro, R.S. 2014. Iron Formation in the Silurian Hills: Relevance to the Evolving Picture of the Neoproterozoic. *In*: Shapiro, R.S., Greene, T.J. & Dehler, C. (eds) *Continental Extension Old and New at the Edge of the Mojave, Book 116*. Pacific Section SEPM (Society for Sedimentary Geology), Upland, CA, 33–39.

Shapiro, R.S., Greene, T.J. & Dehler, C. 2014. *Continental Extension Old and New at the Edge of the Mojave: Book 116*. Pacific Section SEPM (Society for Sedimentary Geology), Upland, CA.

Shastri, L.L., Chamberlain, K.R. & Bowring, S.A. 1991. Inherited zircon from *ca*. 1.1 Ga mafic dikes, NW Arizona (No. 14410). *Geological Society of America, Abstracts with Programs*, **23**, 93.

Smith, D.R., Noblett, J. *et al.* 1999. Petrology and geochemistry of late-stage intrusions of the A-type, mid-Proterozoic Pikes Peak batholith (Central Colorado, USA): implications for petrogenetic models. *Precambrian Research*, **98**, 271–305, https://doi.org/10.1016/S0301-9268(99)00049-2

Smith, E.F., Macdonald, F.A., Crowley, J.L., Hodgin, E.B. & Schrag, D.P. 2016. Tectonostratigraphic evolution of the *c*. 780–730 Ma Beck Spring Dolomite: basin formation in the core of Rodinia. *In*: Li, Z.X., Evans, D.A.D. & Murphy, J.B. (eds) *Supercontinent Cycles Through Earth History*. Geological Society, London, Special Publications, **424**, 213–239, https://doi.org/10.1144/SP424.6

Smith, R.E. & Smith, S.E. 1976. Comments on the use of Ti, Zr, Y, Sr, K, P and Nb in classification of basaltic magmas. *Earth and Planetary Science Letters*, **32**, 114–120, https://doi.org/10.1016/0012-821X(76)90049-2

Stacey, J.S. & Kramers, J.D. 1975. Approximation of terrestrial lead isotope evolution by a two-stage model. *Earth and Planetary Science Letters*, **26**, 207–221, https://doi.org/10.1016/0012-821X(75)90088-6

Sun, S.-S. & McDonough, W. 1989. Chemical and isotopic systematics of oceanic basalts: implications for mantle composition and processes. *In*: Saunders, A.D. & Norry, M.J. (eds) *Magmatism in the Ocean Basins*. Geological Society, London, Special Publications, **42**, 313–345, https://doi.org/10.1144/GSL.SP.1989.042.01.19

Tembo, F., Kampunzu, A.B. & Porada, H. 1999. Tholeiitic magmatism associated with continental rifting in the Lufilian Fold Belt of Zambia. *Journal of African Earth Sciences*, **28**, 403–425, https://doi.org/10.1016/S0899-5362(99)00012-3

Vermeesch, P. 2012. On the visualisation of detrital age distributions. *Chemical Geology*, **312**, 190–194, https://doi.org/10.1016/j.chemgeo.2012.04.021

Vogel, M.B. 2004. *Provenance and Geochemistry of Upper Proterozoic Strata in California and Other Areas of the Western United States: Paleogeographic and Biogeochemical Implications*. PhD thesis, Stanford University, Stanford, CA.

Walker, J.D., Klepacki, D.W. & Burchfiel, B.C. 1986. Late Precambrian tectonism in the Kingston Range, southern California. *Geology*, **14**, 15–18, https://doi.org/10.1130/0091-7613(1986)14<15:LPTITK>2.0.CO;2

Winchester, J. & Floyd, P. 1976. Geochemical magma type discrimination – application to altered and metamorphosed basic igneous rocks. *Earth and Planetary Science Letters*, **28**, 459–469, https://doi.org/10.1016/0012-821X(76)90207-7

Wright, L.A. 1968. *Talc Deposits of the Southern Death Valley–Kingston Range Region, California*. California Division of Mines and Geology, Special Report, **95**.

Yonkee, W.A., Dehler, C.D. *et al.* 2014. Tectono-stratigraphic framework of Neoproterozoic to Cambrian strata, west–central US: Protracted rifting, glaciation, and evolution of the North American Cordilleran margin. *Earth-Science Reviews*, **136**, 59–95, https://doi.org/10.1016/j.earscirev.2014.05.004